# Study of the Reaction $K^+p \to \pi^+ p K^0$ at 12 GeV/$c$ and a Test of the Generalized Veneziano Model at 4.6, 9, and 12 GeV/$c$

Victor Waluch,* Stanley M. Flatté,† and Jerome H. Friedman‡
*Lawrence Berkeley Laboratory, University of California, Berkeley, California 94720*
(Received 7 February 1973)

We present data on the reaction $K^+p \to \pi^+pK^0$ at 12 GeV/$c$, and we present a study of the generalized Veneziano model at 4.6, 9, and 12 GeV/$c$. We have studied the $K^0\pi^+$ mass spectrum and found that in addition to the $K^*(890)$ and $K^*(1420)$ resonances, there is a hint of a resonance at 1.8 GeV, but we were unable to measure its parameters. We have measured the differential cross sections, the total cross sections, the masses and widths, and the spin density matrices of the two $K^*$ and the $\Delta(1236)$ resonances, and find them to be in agreement with previously published data. We have fitted the generalized Veneziano model to our reaction and to data at the other energies. We find that the five parameters used in the theory do not significantly change with energy. The fits at all energies are quite good. However, difficulties with the model at one energy persist at all energies. In particular, we find that the model fits the mass spectra very well at all energies, that the momentum-transfer distributions to the single particles and to the resonances fit well, and that the ratio of the cross sections of resonances in a given channel are well predicted by the model. The model's inability to fit the $p\pi^+$ mass spectrum is evident at all energies.

## I. INTRODUCTION

In the recent past of elementary particle physics there has been a very active search for mathematical models to describe the ever growing empirical knowledge of hadronic phenomena. This search was generally confined to models that would at least in part satisfy some of the postulates of $S$-matrix theory. One of the fruits of this search was the rediscovery by Veneziano of the long dormant Euler beta function. This function was found to possess several of the properties thought to be essential for the descriptions of production processes.[1,2] It has duality, single-Regge limits, crossing, and pole factorization.[3] The generalization of this function by Bardakci and Ruegg and others also possessed multiple-Regge limits. The only glaring shortcoming of this function, the absence of unitarity, though ultimately unacceptable, did not deter phenomenologists from comparing it directly with data in a variety of interactions to see what predictive capacity the model had.[4]

Petersson and Tornqvist were among the first to use the five-point model,[5] as the Bardakci-Ruegg generalization came to be known, in their study of the reaction $K^-p \to \pi^+\pi^-\Lambda$, and Tornqvist[6] used the reaction $\pi^+p \to K^+\pi^+\Lambda$. They reported good over-all fits with only a normalization parameter, albeit many assumptions. Chan, Raitio, Thomas, and Tornqvist[7] (hereinafter referred to as CRTT) undertook the study of the reactions

(i) $K^+p \to \pi^+pK^0$,

(ii) $K^-p \to \pi^-p\overline{K}^0$,

(iii) $\pi^-p \to pK^-K^0$,

which are related by crossing, and Bartsch *et al.*[8] made a study of reaction (ii). Raitio[9] subsequently studied the reactions

(iv) $K^+n \to K^0\pi^+n$,

(v) $K^-n \to \overline{K}^0\pi^-n$,

related to (i)–(iii) by isospin invariance. These studies reported that an adequate fit to the data in the various channels could be obtained from a simple model with the over-all normalization as the only free parameter. Cross sections, as well as the various experimental distributions available in the three-particle final state, were fitted with no new parameters.

Such a global success with so few adjustable parameters at first seemed impressive, especially when compared with other models that have much more inherent freedom but fail to do better. However, a closer look at the above works showed that to some degree the quality of the fits reflected a judicious input into the model, so it became evident that the claims of one-parameter fits were somewhat misleading. In an earlier work[10] we had undertaken a detailed test of the Bardakci-Ruegg model to the data of reaction (i) in order to determine what portions of the successes of the model are truly independent of the input. We have shown that even without *ad hoc* modification of trajectory functions, a good fit may be obtained but at the expense of using several kinematic factors and five adjustable parameters.

The purpose of this paper is twofold. First, we present the results of our experiment on the reaction $K^+p \to \pi^+pK^0$ at 12 GeV/$c$. In Sec. II we discuss the importance of this reaction, the gath-

ering of the data, the scanning, measuring, and fitting procedures, and their associated biases and efficiencies. In Sec. III we present the cross sections and studies of final-state resonances and their decays. Second, we extend our earlier study of the Bardakci-Ruegg function to lower energies. We discuss the formulation of our model and our assumptions. We include discussions of the computer programs used in our calculations, and we present the results of our calculations in a large set of histograms.

## II. THE DATA

### A. Introduction

The data, 1901 events, come from 600 000 pictures exposed to a radio-frequency separated $K^+$ meson beam at 11.9 GeV/$c$ in the SLAC 82 in. hydrogen bubble chamber.[11,12] The photographs were scanned and measured by the Group A Scanning and Measuring Group at the Lawrence Berkeley Laboratory. Film measurement was done on the Spiral Reader II semiautomatic measuring machine. Reduction and analysis of the data were done on the CDC 6600 computer by means of the standard Group A analysis programs: POOH, TVGP and SQUAW.

### B. Scanning, Measuring, and Fitting Procedures

Our reaction topology, two prongs and a $V$, corresponding to the decay of a neutral particle, was searched for in a general scan of the film which recorded all $K^+$-induced reactions. The scan criteria for our topology were quite loose: The $V$ had to point back to the production vertex within a generous tolerance, and had to have a nonzero opening angle (to distinguish it from $e^+e^-$ pairs). In cases of doubt, the scanners were instructed to include the event in the sample. This procedure prevented the introduction of possible scanning biases as well as prevented the premature loss of events. All rolls were scanned twice, and some ten percent of the rolls were scanned three times. Any conflicts between the two scans were resolved by an independent conflict scan.

The odd rolls of film had three measurement passes, and the even rolls had two. Events failing on the first and second measurement passed as nonbeam events and were not measured the third time. Events failing three times were looked at on the scan table by physicists to determine if there were any systematic biases.

The two-prong $V$ topology events were fitted to the following four-constraint reactions:

(i) $K^+p \to \pi^+ pK^0$,

(ii) $K^+p \to K^+K^+\Lambda$,

(iii) $K^+p \to pp\bar{\Lambda}$.

In addition, many one- and zero-constraint reactions were fitted.

In the above fits, the $V$ was first fitted to the reactions

(i) $K^0 \to \pi^+\pi^-$,

(ii) $\Lambda \to p\pi^-$,

(iii) $\bar{\Lambda} \to \bar{p}\pi^+$,

using the production vertex as the source of the neutral. This resulted in a three-constraint fit. If a three-constraint fit did not work, a one-constraint fit was attempted.

### C. Scanning and Measuring Biases and Efficiencies

Scanning biases occur in three main ways: misidentification of a $K^0$ decay with an $e^+e^-$ pair, so that the event is not recorded, misinterpretation of a two-prong $V$ event as a four-prong when the $K^0$ decays too close to the production vertex, and failure to recognize the topology when the recoil proton track is very short. In the first case, we have looked at the angle between the outgoing positive track and the direction of the $K^0$. In the $K^0$ rest frame this angle should be flat, and this was found to be so. In the second case, we have looked at the distribution of the decay lengths of the $K^0$ and have found that for lengths less than 6 mm, there was a marked bias. Consequently we have made a cut on events for which the decay length was less than 6 mm. The remaining events were weighted by the factor $\exp(x/\eta c\tau)$, where $x$ is the $K^0$ cutoff (=6 mm) and $\eta$ is the laboratory momentum of the $K^0$ in GeV/$c$ divided by the mass of the $K^0$ in GeV$^2$, and $\tau$ is the mean life of the $K^0$. The third bias was studied in the following way. We took all the two-prong $V$ events that had a fit to any hypothesis. We then looked at the results of the two scans and the conflict scan. Using the usual expressions, we could derive the detection probability of a two-prong $V$ event as a function of the length of its positive track at the production vertex. We repeated this exercise choosing only those events fitting our reaction, and found that the results agreed with the results of the larger sample, as was expected. Figure 1(a) shows the detection probability after two scans as a function of the proton track length. As may be seen, a bias exists only for proton track lengths less than 1 cm. Each event was weighted by the inverse of its detection probability as given by Fig. 1(a). Finally, we checked for systematic biases due to measuring by comparing angular distributions at the production and decay vertices of events that passed on

the first measurement pass with those that failed the first but passed the second and with those that pass only on the third pass. To within statistical errors, no systematic bias could be detected.

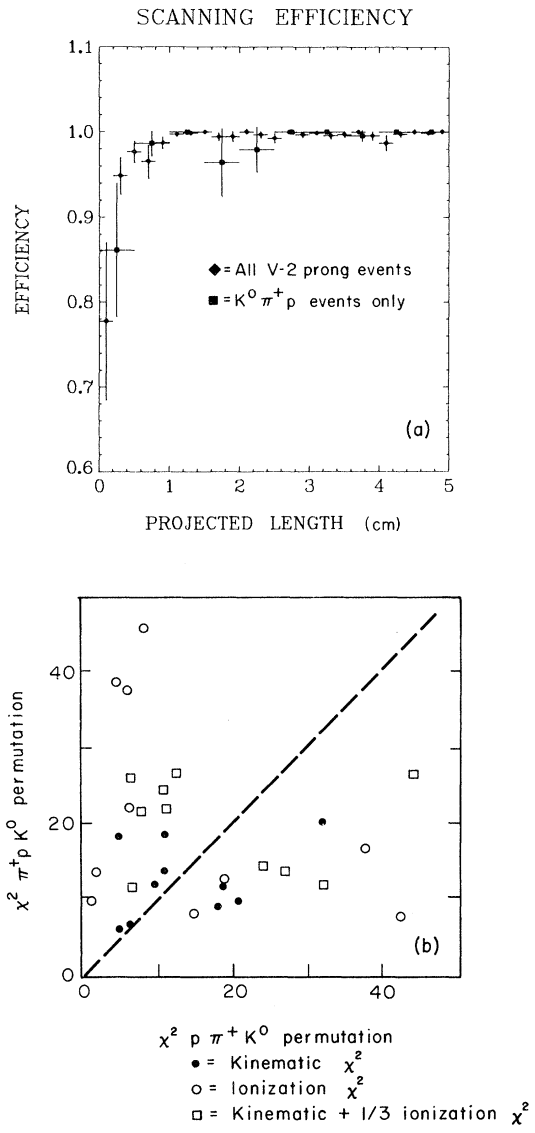


FIG. 1. (a) Film scanning efficiency for our event type as a function of the recoil proton track length. After two scans the over-all efficiency is nearly 100%. However, for small recoil lengths there is a marked bias so a correction was done. The triangular points represent the scanning efficiency for all $V$-two prongs irrespective. of reaction type. The square points are for our reaction only. The square points have larger errors since the statistics were smaller. The two scanning efficiencies are the same to within errors. (b) Fitted $\chi^2$ for events ambiguous under $p \leftrightarrow \pi^+$ permutation. The sum of ionization and kinematic $\chi^2$ shows a clear separation of the events.

### D. Ambiguities

An event was considered as passing if it fitted the kinematics of our reaction with a confidence level of $10^{-5}$. Experience has shown that if a four-constraint hypothesis fits within this criterion, then it is highly probable that the hypothesis is true even though the event may fit a less constrained hypothesis with a better confidence level. Thus, we ignored a less constrained hypothesis. There still remained the possibility that our events fitted other four-constraint hypotheses, namely, reactions (ii) and (iii). Investigation showed that there was only one such ambiguous event at $10^{-5}$ confidence level. Its kinematics fits reactions (i) and (iii) equally well. However, the ionization information available from the Spiral Reader II favored reaction (i), so the event was left in the sample as fitting reaction (i). Another possible source of ambiguity is within reaction (i) itself. It arises from the possibility of the proton and the $\pi^+$ faking each other. Ten such cases occurred. Of these ten, six had kinematic confidence levels differing by at least 50%; the other four had nearly identical confidence levels. However, ionization information clearly separated the events. Figure 1(b) shows the kinematic $\chi^2$, the ionization $\chi^2$, and the sum.[13] As can be seen, a separation is strongly suggested. Therefore, we assigned these events to the reaction for which its kinematic $\chi^2$ plus $\frac{1}{3}$ its ionization $\chi^2$ were smaller. Thus, we can say with a high degree of confidence that our data are exceedingly free from contamination by other reactions or by permutation of tracks within the reaction itself.

## III. EXPERIMENTAL RESULTS

### A. Total Cross Sections

#### 1. *Path Length*

The path length of our experiment was determined by three independent methods[14]: $\tau$-decay method, beam tally method, and by normalization to the total cross section. The procedures are too lengthy to discuss here. The interested reader may check Ref. 15 for further details. Table I shows the results of the three methods. The weighted average of the three methods is $34.9 \pm 0.5$ events/$\mu$b.

#### 2. *Scanning Efficiency*

Figure 1(a) shows the scanning efficiency as a function of the proton length. Each event in our reaction was weighted by the inverse of its detection probability as obtained from this figure. This consideration had only a 0.4% effect on the total cross section.

TABLE I. Summary of the three methods of determining the path length. The average had a $\chi^2$ of 0.8 with 3 degrees of freedom, corresponding to a confidence level of about 80%.

| Method | Path length (events/$\mu$b) | Average (events/$\mu$b) |
|---|---|---|
| $\tau$ decays | $34.7 \pm 0.9$ | |
| Beam track tally | $35.2 \pm 0.6$ | |
| Normalization to total cross section | $34.0 \pm 1.2$ | $34.9 \pm 0.5$ |

### 3. *Measuring Efficiency*

The measuring efficiency for our reaction is $0.846 \pm 0.026$. No measurement bias was found. Further details may be found in Ref. 16.

### 4. *$K_S^0$ Decay Length*

As discussed in Sec. II D, events whose $K^0$ decayed within 6 mm of the production vertex were discarded and the rest of the events were weighted by the factor $\exp(x/\eta c\tau)$. Since the bubble chamber is not infinite in size, the events were weighted by a factor describing the decay probability of the $K^0$ within a preselected fiducial volume of the bubble chamber. These two combined weightings revised the cross section upwards by the factor 1.27.

### 5. *$K^0$ Branching Ratio*

Since the $K^0$ decays into the detected $\pi^+\pi^-$ $(68.7 \pm 0.5)/2$ percent of the time, the cross sections were multiplied by the inverse of this branching ratio.

### 6. *$K_L^0$ Decays*

The $K_L^0$ decays into $\pi^+\pi^-\pi^0$ present no problem since they are only a $0.4 \pm 0.04\%$ correction to the cross section.

The cross sections were determined by the formula

$$\sigma = W \times (1/P) \times (1/B), \tag{1}$$

where

$W$ = the expected number of events,

$P$ = the path length,

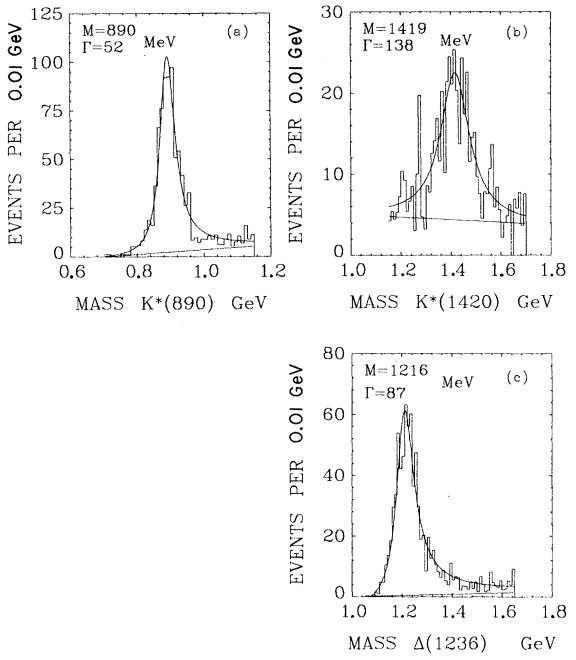


FIG. 2. (a) Fit of the $K^*(890)$ region. The mass and width were varied, and a linear approximation to the background was used. (b) Fit of the $K^*(1420)$ region. The mass and width were varied, and a linear approximation to the background was used. (c) Fit of the $\Delta(1236)$ region. The mass and width were varied, and a linear approximation to the background was used.

and

$B$ = $K^0$ branching ratio into $\pi^+\pi^-$.

The term $W$ is equal to

$$W = N_{\text{obs}}/E, \tag{2}$$

where

$N_{\text{obs}}$ = number of observed events,

and

$E$ = product of the efficiencies of 2, 3, 4, and 6 above.

The results of these calculations are shown in Table II.

TABLE II. 12-GeV/$c$ measurements.

| Type | Cross section ($\mu$b) | No. events | $M$ (MeV) | $\Gamma$ (MeV) |
|---|---|---|---|---|
| All events | $238.6 \pm 11$ | $2419 \pm 50$ | | |
| $K^*(890)$ | $78.3 \pm 3.9$ | $794 \pm 21$ | 889.5(+1.5, −1.5) | 52.4(+3.5, −3.3) |
| $K^*(1420)$ | $32.8 \pm 4.5$ | $333 \pm 40$ | 1419.0(+7.6, −7.6) | 138.4(+28.9, −23.4) |
| $\Delta(1236)$ | $75.0 \pm 4.2$ | $761 \pm 26$ | 1216.0(+3.4, −3.3) | 87.5(+6.4, −5.9) |
| $K^*(1850)$ | $<18 \pm 50\%$ | | | |
| $Z^*(1800)$ | $<2 \pm 50\%$ | | | |

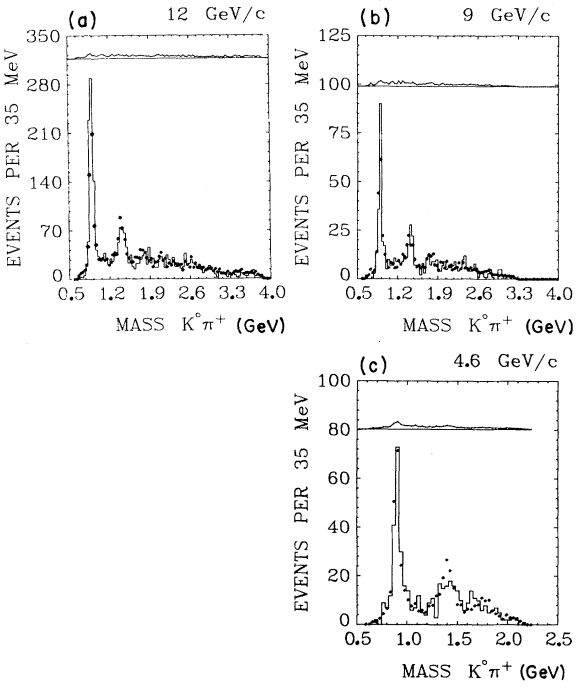


FIG. 3. Invariant mass of $K^0\pi^+$. The fits at 12 and 9 GeV/$c$ are quite good, as is the fit at 4.6 GeV/$c$. It should be noted that the $K^*(890)$ at 9 GeV/$c$ in the data is only some 35 MeV wide, much less than the accepted width of 50 MeV.

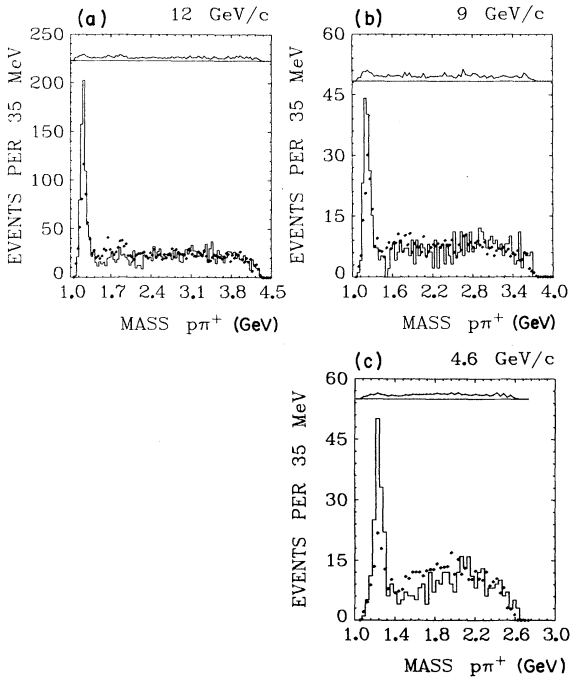


FIG. 4. Invariant mass of $p\pi^+$. The over-all fit is reasonable at all energies. However, the fits to the $\Delta(1236)$ region are poor at all energies, especially at 4.6 GeV/$c$.

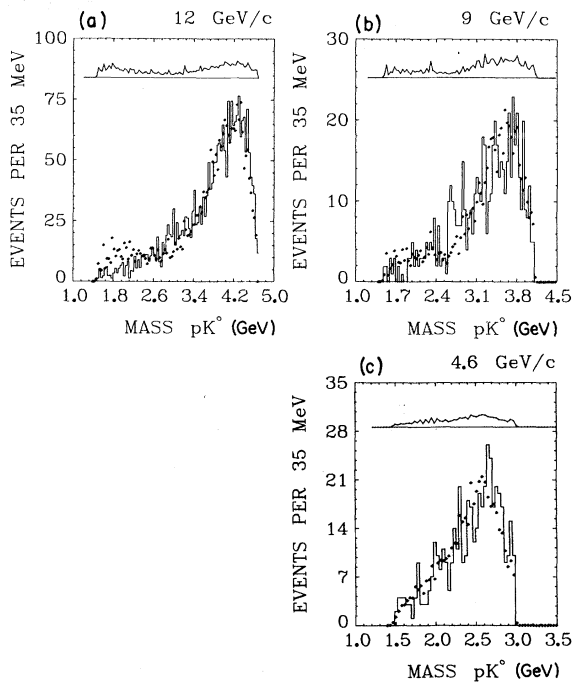


FIG. 5. Invariant mass of $pK^0$. The fits at all energies are excellent, supporting the idea of the absence of exotic resonances in this channel.

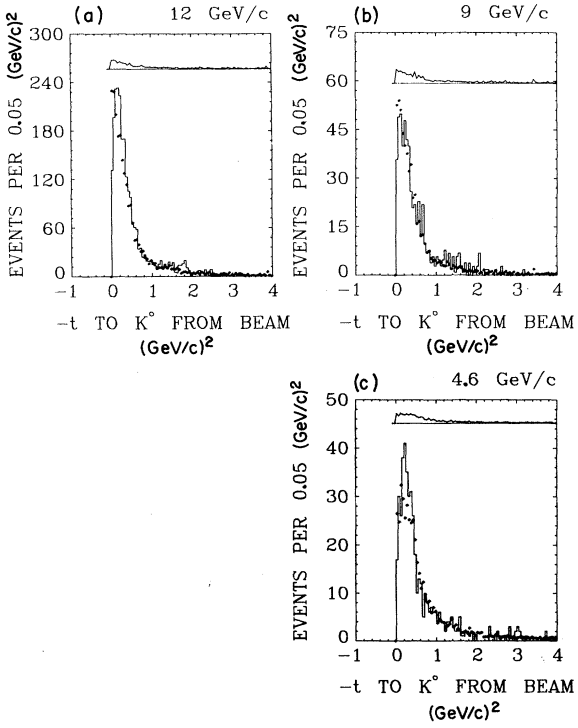


FIG. 6. $-t$ to $K^0$ from beam. Except for the forward few bins, the fits are good at all energies up to the highest allowed values of $-t$.

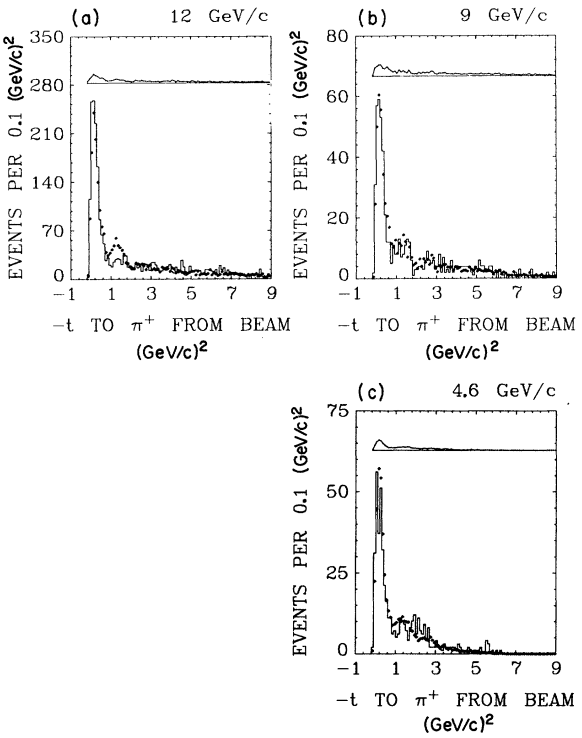


FIG. 7. $-t$ to $\pi^+$ from beam. The fits are quite good except for the bump at $-1$ $(\mathrm{GeV}/c)^2$.

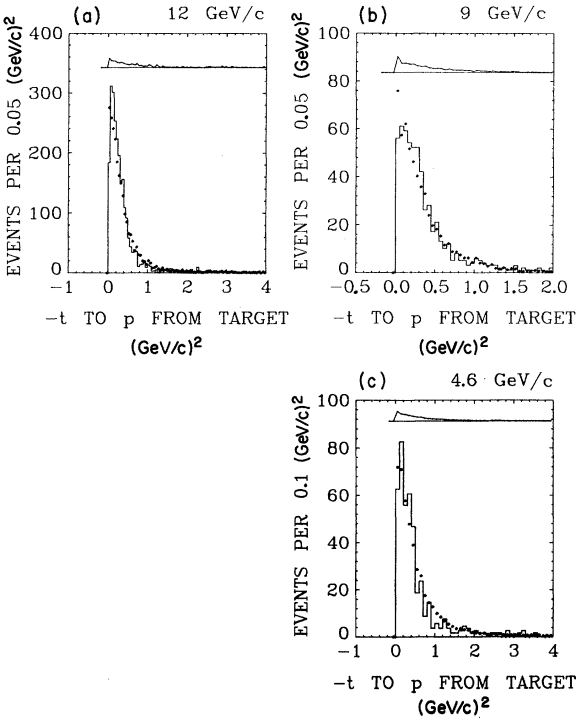


FIG. 8. $-t$ to $p$ from target. Except for the forward bins, the fits are good.

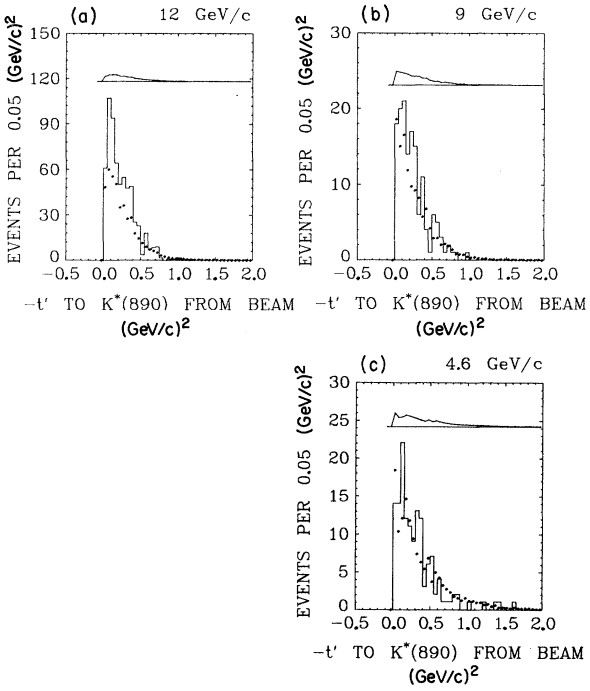


FIG. 9. $-t'$ to $K^*(890)$ from beam. Apart from normalization, the fits are good. Inadequacy of our handling of pion exchange is obvious in the 4.6-GeV/$c$ data, where the peaking of the theory in the forward direction is very pronounced but the data turn over. The pion contribution is nearly all in the first bin.

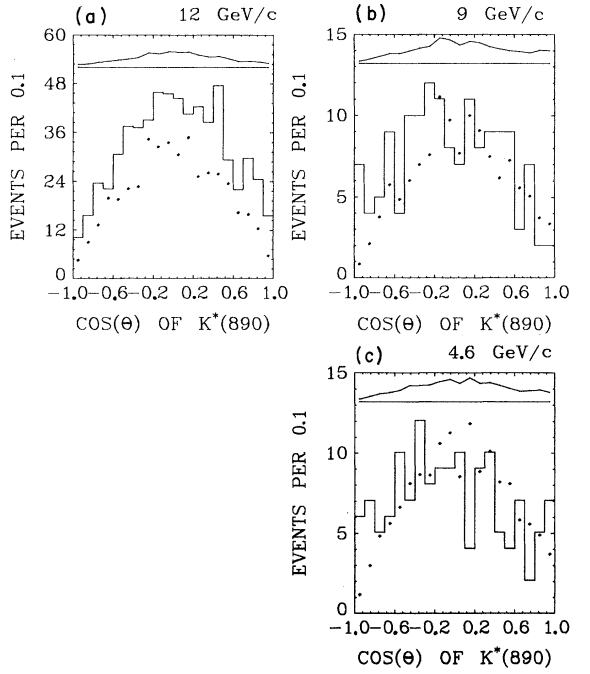


FIG. 10. $\cos\theta$ of $K^*(890)$ in the Jackson frame. The fits at all energies are reasonable.

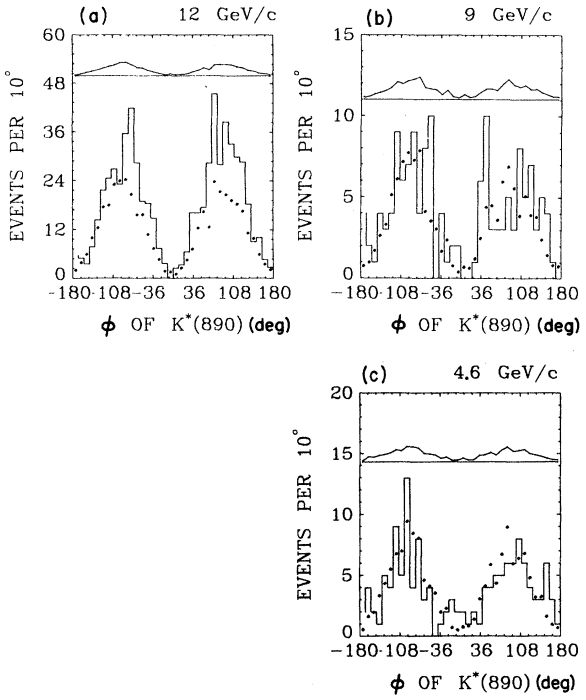


FIG. 11. $\phi$ of $K^*(890)$ in the Jackson frame. The fits at all energies are quite good.

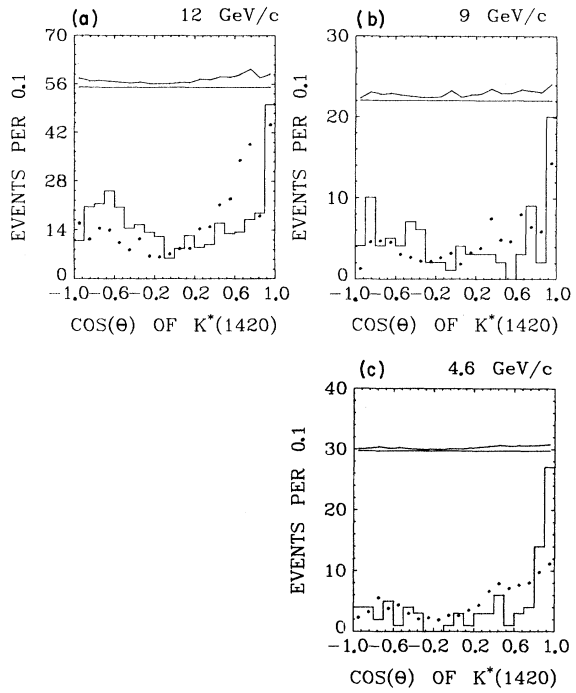


FIG. 13. cos$\theta$ of $K^*(1420)$ in the Jackson frame. The theory tends to follow the trend of the data, but the fits are not good. In particular, the interference of the $K^*$ with the $\Delta$ in the rightmost bin is not well reproduced in the 4.6-GeV/$c$ data.

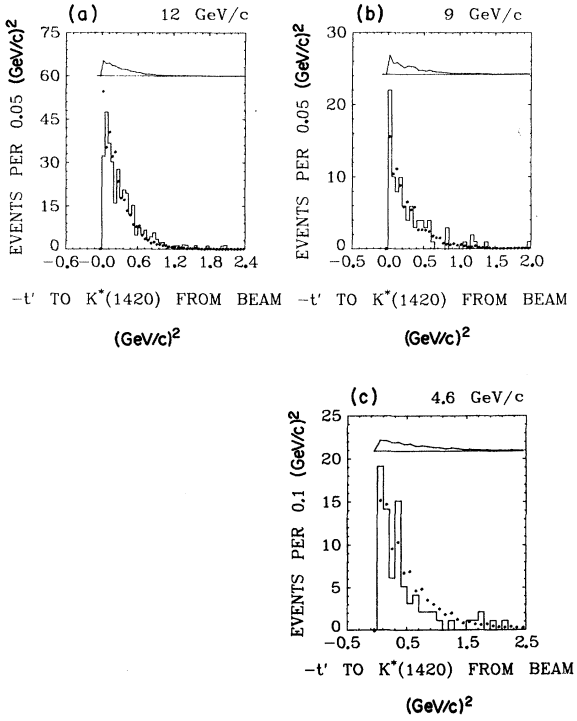


FIG. 12. $-t'$ to $K^*(1420)$. Except for the first few bins, the fits are reasonable.

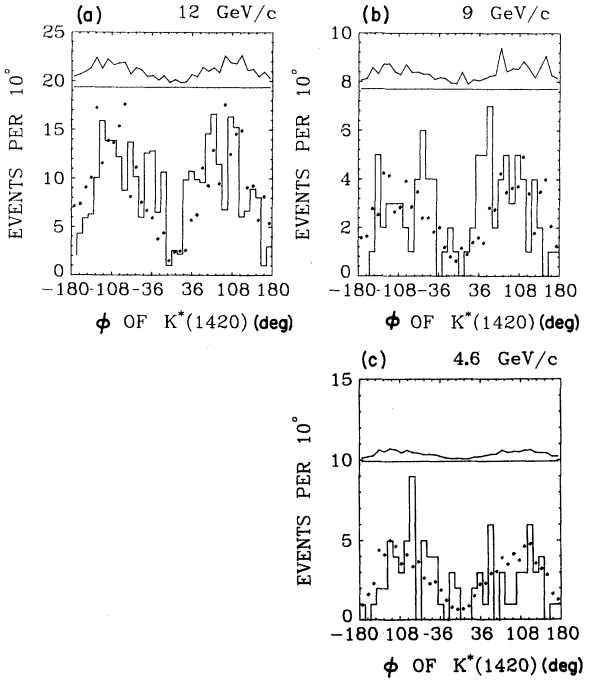


FIG. 14. $\phi$ of $K^*(1420)$ in the Jackson frame. The fits at all energies are quite good.

### B. Resonances and Their Decays

#### 1. *Prominent Resonances*

The prominent feature of our data is the copious production of the three resonances: $K^*(890)$ $J^P = 1^-$, $K^*(1420)$ $J^P = 2^+$, and $\Delta(1236)$ $J^P = \frac{3}{2}^+$, which account for some $\frac{3}{4}$ of the data. Further discussion of these resonances is reserved for Sec. IV, where we compare the experimental detail with the predictions of the theory. In this section we present experimental measurements of resonance parameters, cross sections, and the spin-density matrix elements of the resonances.

We performed a fit to each prominent resonance using the standard Breit-Wigner line shape as given by Jackson.[17] We allowed for nonresonant background by including a linear approximation for the background in the fit. We let the masses, widths, slopes and intercepts of the background, as well as the relative amounts of resonance to background be variable. The fits were done using the maximum-likelihood method. Table II shows the results of the fits. The cross sections were calculated as discussed in Sec. III. Figures 2(a), 2(b), and 2(c) display the fitted line shapes to the resonances, the background, and the data.

We have also fitted the spin-density matrix elements of each resonance. For the $K^*(890)$ we used the following expression:

$$W_{K^*(890)}(\theta,\phi) = C[\rho_{11}\sin^2\theta + (1-2\rho_{11})\cos^2\theta - \rho_{1,-1}\sin^2\theta\cos 2\phi - \sqrt{2}\,\mathrm{Re}\rho_{10}\sin 2\theta\cos\phi]. \tag{3}$$

The $K^*(1420)$ was fitted to the formula

$$\begin{aligned} W_{K^*(1420)}(\theta,\phi) = C\{&\rho_{11}[-6(\cos^2\theta-\tfrac{1}{3})^2 + 4\sin^2\theta\cos^2\theta] + \rho_{22}[\sin^4\theta - 6(\cos^2\theta-\tfrac{1}{3})^2] \\ &- 2\cos\phi\sin 2\theta[(\mathrm{Re}\rho_{21}\sin^2\theta + \sqrt{6}\,\mathrm{Re}\rho_{10}(\cos^2\theta-\tfrac{1}{3})] \\ &- 2\cos 2\phi\sin^2\theta[2\rho_{1-1}\cos^2\theta - \sqrt{6}\,\mathrm{Re}\rho_{20}(\cos^2\theta-\tfrac{1}{3})] \\ &+ 2\,\mathrm{Re}\rho_{2-1}\cos 3\phi\sin 2\theta\sin^2\theta + \rho_{2-2}\cos 4\phi\sin^4\theta\}, \end{aligned} \tag{4}$$

and $\Delta(1236)$ was fitted to the formula

$$\begin{aligned} W_{\Delta(1236)}(\theta,\phi) = C\Big[&\rho_{33}\sin^2\theta + (\tfrac{1}{2}-\rho_{33})(\tfrac{1}{3}+\cos^2\theta) \\ &- \frac{2}{\sqrt{3}}\mathrm{Re}\rho_{3,-1}\sin^2\theta\cos 2\phi \\ &- \frac{2}{\sqrt{3}}\mathrm{Re}\rho_{31}\sin 2\theta\cos\phi\Big]. \end{aligned} \tag{5}$$

In the above expressions, $C$ is just a normalization constant.

Where there were sufficient numbers of events, we performed the fits for various mass cuts and various $-t'$ cuts. $-t'$ is defined as usual: $-t' = -(t - t_{\min})$. Momentum transfer distributions to the single particles and to the resonances are shown among Figs. 3–17. Tables III–V show the results. The first set of entries in these tables is for fixed-mass cut of plus or minus a resonance width about the central mass with $-t'$ cuts as shown. The second set of entries has no momentum transfer cuts but has the following mass cuts: (1) mass within ± two resonance widths of the central mass, (2) mass within one resonance width of the central mass, (3) mass within one resonance width below the central value, and (4) mass within one resonance width above the central value. The third set of entries is for mass cuts in bands of various sizes starting on the low-mass side of the resonance and marching through to the high side of the resonance. Figure 18 shows a plot of the density matrix elements for the $K^*(890)$ as a function of the invariant four-momentum transfer. The

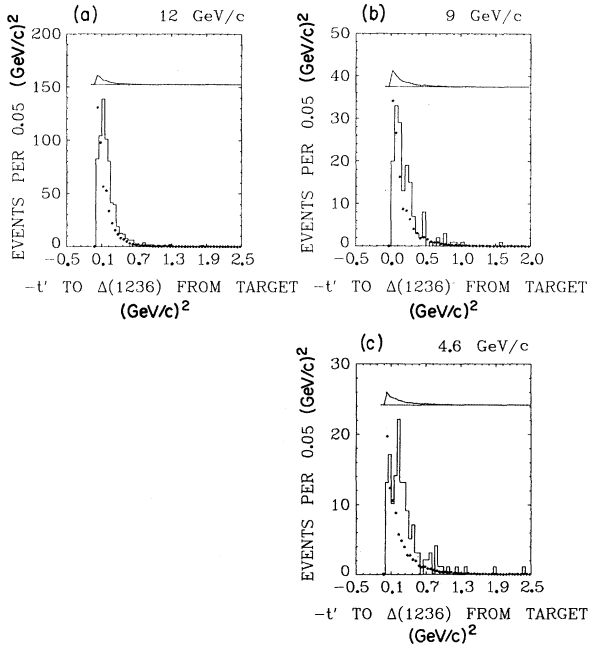


FIG. 15. $-t'$ to $\Delta(1236)$ from target. The fits are poor at all energies.

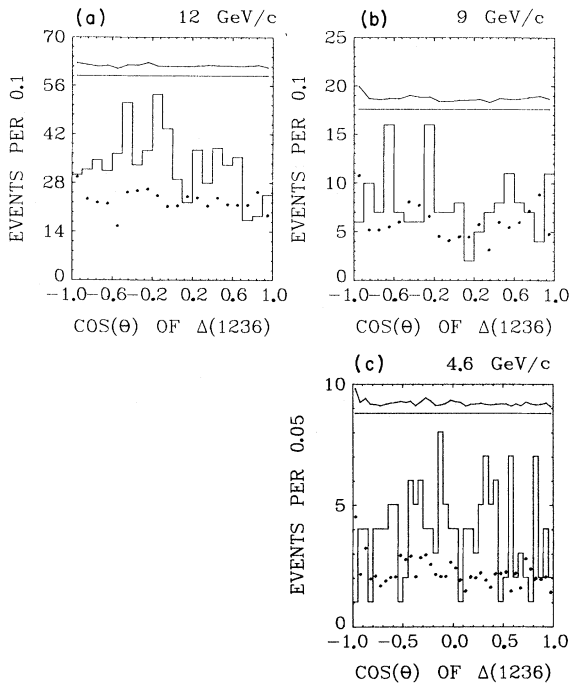


FIG. 16. $\cos\theta$ of $\Delta(1236)$ in the Jackson frame. The theory has a large $L = 0$ component which approximates the data. However, there is some $\cos^2\theta$ distribution in the 12-GeV/$c$ data that does not appear in the theory.

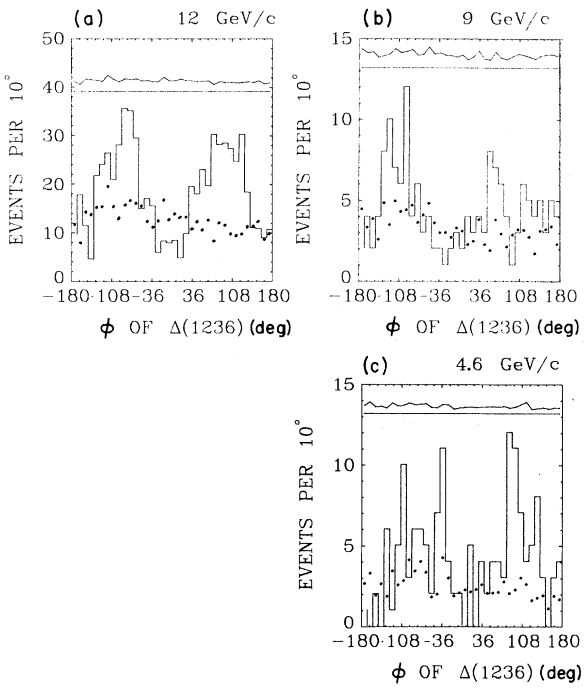


FIG. 17. $\phi$ of $\Delta(1236)$ in the Jackson frame. The fits are poor at all energies because the theory is nearly all $L = 0$ and the data is not.

value of $\rho_{00}$ peaks in the small momentum region and dies away rapidly with increasing momentum transfer. The value of $\rho_{11}$, on the other hand, starts small and grows. This behavior indicates pseudoscalar exchange at small momentum transfer. This phenomenon indicates the necessity of including pion exchange in any model that attempts to fit the differential cross section of the $K^*$ resonances in the forward direction. Figure 19 shows a similar plot of the density matrix elements of the $\Delta(1236)$. The values of the density matrix elements for the $\Delta(1236)$ are consistent with the model of Stodolsky and Sakurai as shown in Table V. Since the background under the $K^*(1420)$ is large, we attempted to estimate its contribution to the spin-density matrix elements of $K^*(1420)$ by fitting the matrix elements to mass regions where the background dominates. We chose two such cuts in the wings on both sides of the resonance. We then estimated the contribution of the background

TABLE III. Density matrix fits $K^*(890)$.

| Mass cut (MeV) | $t$ cut [(GeV/$c$)$^2$] | No. | $\rho_{00}$ | $\rho_{1-1}$ | Re$\rho_{10}$ |
|---|---|---|---|---|---|
| $839 \le M \le 943$ | $0.0 \le -t \le 0.10$ | 115 | $0.237 \pm 0.070$ | $0.357 \pm 0.045$ | $0.046 \pm 0.025$ |
| $839 \le M \le 943$ | $0.10 \le -t \le 0.20$ | 108 | $0.089 \pm 0.052$ | $0.517 \pm 0.042$ | $-0.013 \pm 0.033$ |
| $839 \le M \le 943$ | $0.20 \le -t \le 0.30$ | 85 | $-0.037 \pm 0.062$ | $0.455 \pm 0.052$ | $-0.098 \pm 0.033$ |
| $839 \le M \le 943$ | $0.30 \le -t \le$ all | 151 | $-0.075 \pm 0.021$ | $0.517 \pm 0.025$ | $-0.013 \pm 0.019$ |
| $787 \le M \le 995$ | No cut | 559 | $0.097 \pm 0.022$ | $0.435 \pm 0.017$ | $0.003 \pm 0.011$ |
| $839 \le M \le 943$ | No cut | 459 | $0.076 \pm 0.023$ | $0.445 \pm 0.017$ | $-0.001 \pm 0.011$ |
| $839 \le M \le 891$ | No cut | 220 | $0.057 \pm 0.023$ | $0.479 \pm 0.021$ | $0.004 \pm 0.018$ |
| $891 \le M \le 943$ | No cut | 239 | $0.095 \pm 0.036$ | $0.416 \pm 0.028$ | $-0.003 \pm 0.017$ |
| $839 \le M \le 859$ | No cut | 36 | $0.022 \pm 0.057$ | $0.748 \pm 0.088$ | $-0.079 \pm 0.039$ |
| $859 \le M \le 879$ | No cut | 119 | $0.018 \pm 0.036$ | $0.465 \pm 0.040$ | $0.003 \pm 0.021$ |
| $879 \le M \le 899$ | No cut | 140 | $0.147 \pm 0.054$ | $0.473 \pm 0.030$ | $0.022 \pm 0.016$ |
| $899 \le M \le 919$ | No cut | 100 | $0.091 \pm 0.054$ | $0.391 \pm 0.049$ | $0.028 \pm 0.035$ |
| $919 \le M \le 939$ | No cut | 65 | $0.046 \pm 0.071$ | $0.436 \pm 0.043$ | $-0.036 \pm 0.027$ |

TABLE IV. Density matrix fits $K^*(1420)$.

| Mass cut (MeV) | $t$ cut $[(\mathrm{GeV}/c)^2]$ | No. | $\rho_{11}$ | $\rho_{22}$ | $\mathrm{Re}\rho_{21}$ | $\mathrm{Re}\rho_{20}$ | $\mathrm{Re}\rho_{2-1}$ | $\rho_{2-2}$ | $\mathrm{Re}\rho_{10}$ | $\rho_{1-1}$ |
|---|---|---|---|---|---|---|---|---|---|---|
| $1302 \leq M \leq 1542$ | $0.0 \leq -t \leq 0.50$ | 212 | $0.267 \pm 0.028$ | $0.025 \pm 0.031$ | $0.185 \pm 0.018$ | $0.026 \pm 0.018$ | $0.101 \pm 0.023$ | $-0.117 \pm 0.032$ | $0.037 \pm 0.028$ | $0.203 \pm 0.034$ |
| $1182 \leq M \leq 1662$ | No cut | 411 | $0.247 \pm 0.020$ | $0.051 \pm 0.023$ | $0.133 \pm 0.015$ | $0.051 \pm 0.015$ | $0.082 \pm 0.016$ | $-0.105 \pm 0.024$ | $0.048 \pm 0.024$ | $0.139 \pm 0.025$ |
| $1302 \leq M \leq 1542$ | No cut | 282 | $0.276 \pm 0.023$ | $0.065 \pm 0.027$ | $0.162 \pm 0.017$ | $0.024 \pm 0.016$ | $0.102 \pm 0.023$ | $-0.123 \pm 0.030$ | $0.035 \pm 0.024$ | $0.210 \pm 0.030$ |
| $1302 \leq M \leq 1422$ | No cut | 156 | $0.298 \pm 0.029$ | $0.049 \pm 0.035$ | $0.147 \pm 0.023$ | $0.021 \pm 0.020$ | $0.086 \pm 0.032$ | $-0.108 \pm 0.038$ | $0.052 \pm 0.031$ | $0.227 \pm 0.040$ |
| $1422 \leq M \leq 1542$ | No cut | 126 | $0.191 \pm 0.037$ | $0.078 \pm 0.041$ | $0.248 \pm 0.027$ | $0.078 \pm 0.031$ | $0.110 \pm 0.034$ | $-0.237 \pm 0.063$ | $-0.080 \pm 0.038$ | $0.207 \pm 0.037$ |
| $1352 \leq M \leq 1402$ | No cut | 68 | $0.297 \pm 0.047$ | $0.081 \pm 0.051$ | $0.152 \pm 0.043$ | $0.015 \pm 0.035$ | $0.137 \pm 0.058$ | $-0.101 \pm 0.059$ | $0.039 \pm 0.045$ | $0.235 \pm 0.064$ |
| $1402 \leq M \leq 1452$ | No cut | 85 | $0.309 \pm 0.043$ | $0.136 \pm 0.045$ | $0.216 \pm 0.037$ | $-0.015 \pm 0.028$ | $0.107 \pm 0.047$ | $-0.135 \pm 0.065$ | $0.010 \pm 0.047$ | $0.207 \pm 0.065$ |
| $1370 \leq M \leq 1470$ | No cut, background corrected | | $0.276 \pm 0.04$ | $0.134 \pm 0.05$ | $0.185 \pm 0.04$ | $-0.044 \pm 0.03$ | $0.122 \pm 0.04$ | $-0.077 \pm 0.06$ | $0.617 \pm 0.05$ | $0.0246 \pm 0.06$ |

to the matrix elements at the center of the resonance by averaging these two fits for each element. The matrix elements fitted to the central area of the resonance were then corrected by subtracting off the contribution of the background. The contribution of the background was assumed to be the average of the above fits multiplied by the fraction of background events in the region. The results are shown in the final entries in Table IV.

### 2. *Other Resonances*

There has been a suggestion of a possible resonance in the 1.85-GeV region of the $K\pi$ mass spectrum. Firestone *et al.*[18] have studied this mass region in the reaction $K^+n \to K^+\pi^-p$ at 12 GeV/$c$ and have presented evidence in support of a possible assignment of $J^p = 3^-K^*$ resonance interpretation for this mass region. We have looked at this mass region in our data. Figure 20(a) shows a plot of the mass of the $K\pi$ mass system versus the cosine of the $K\pi$ decay angle in the Jackson frame. Figure 20(b) shows a similar plot but with a cut of $-t'$ less than 0.2 on the invariant four-momentum transfer to the $K\pi$ system. If we assume a mass of 1.85 GeV, a width of 300 MeV, and a background of 50%, we get by a simple event count an upper bound on the cross section of 18 $\mu$b for this resonance in our reaction.

We have also investigated the presence of a $K^0p$ exotic resonance at 1.8 GeV. To enhance the signal in this channel, we made the following cuts. In the rest frame of the outgoing $K^0$ and the outgoing proton, we chose events such that the directional cosine between the $K^0$ and the beam was negative. This cut removed a large part of the $K^*$ and $\Delta$ events since they tend to have the $K^0$ aligned parallel with the beam direction. This cut also removed about one-half of the signal. Assuming a mass of 1.8 GeV and a width of 300 MeV, a direct event count corrected for the cuts yielded 20 events for the resonance. No peaking of events in this mass region was observed, and the upper bound on the cross section for such a resonance in this mass region is 2 $\mu$b.

## IV. A TEST OF THE GENERALIZED VENEZIANO MODEL

### A. Introduction

Since the realization by physicists of the remarkable properties of the Euler beta function, many phenomenologists have attempted to fit the function to two-particle-in and two-particle-out reactions (henceforth to be called four-point reaction; similarly, two-in and three-out will be called five-point, etc.). Following the early qual-

TABLE V. Density matrix fits Δ(1236).

| Mass cut (MeV) | $t$ cut [(GeV/$c$)$^2$] | No. | $\rho_{33}$ | Re$\rho_{3-1}$ | Re$\rho_{31}$ |
|---|---|---|---|---|---|
| $1116 \le M \le 1356$ | $0.0 \le -t \le 0.10$ | 118 | $0.368 \pm 0.049$ | $0.171 \pm 0.054$ | $-0.065 \pm 0.044$ |
| $1116 \le M \le 1356$ | $0.10 \le -t \le 0.20$ | 159 | $0.331 \pm 0.043$ | $0.253 \pm 0.042$ | $0.045 \pm 0.040$ |
| $1116 \le M \le 1356$ | $0.20 \le -t \le 0.30$ | 80 | $0.366 \pm 0.061$ | $0.184 \pm 0.063$ | $-0.074 \pm 0.056$ |
| $1116 \le M \le 1356$ | $0.30 \le -t \le 0.40$ | 34 | $0.440 \pm 0.066$ | $0.215 \pm 0.110$ | $0.347 \pm 0.088$ |
| $1116 \le M \le 1356$ | $0.40 \le -t \le$ all | 39 | $0.381 \pm 0.074$ | $0.223 \pm 0.104$ | $-0.109 \pm 0.100$ |
| $996 \le M \le 1476$ | No cut | 482 | $0.333 \pm 0.024$ | $0.209 \pm 0.025$ | $0.018 \pm 0.024$ |
| $1116 \le M \le 1356$ | No cut | 430 | $0.357 \pm 0.025$ | $0.219 \pm 0.027$ | $-0.008 \pm 0.025$ |
| $1116 \le M \le 1236$ | No cut | 269 | $0.344 \pm 0.032$ | $0.236 \pm 0.031$ | $-0.041 \pm 0.029$ |
| $1236 \le M \le 1356$ | No cut | 161 | $0.384 \pm 0.044$ | $0.192 \pm 0.048$ | $0.047 \pm 0.040$ |
| $1136 \le M \le 1156$ | No cut | 19 | $0.050 \pm 0.145$ | $0.106 \pm 0.139$ | $-0.013 \pm 0.116$ |
| $1156 \le M \le 1176$ | No cut | 36 | $0.362 \pm 0.096$ | $0.299 \pm 0.086$ | $-0.272 \pm 0.095$ |
| $1176 \le M \le 1196$ | No cut | 55 | $0.304 \pm 0.079$ | $0.237 \pm 0.067$ | $-0.014 \pm 0.061$ |
| $1196 \le M \le 1216$ | No cut | 71 | $0.374 \pm 0.056$ | $0.289 \pm 0.058$ | $-0.007 \pm 0.053$ |
| $1216 \le M \le 1236$ | No cut | 82 | $0.414 \pm 0.048$ | $0.232 \pm 0.059$ | $-0.045 \pm 0.055$ |
| $1236 \le M \le 1256$ | No cut | 53 | $0.391 \pm 0.073$ | $0.154 \pm 0.079$ | $-0.006 \pm 0.069$ |
| $1256 \le M \le 1276$ | No cut | 39 | $0.416 \pm 0.073$ | $0.236 \pm 0.104$ | $0.078 \pm 0.080$ |
| $1276 \le M \le 1296$ | No cut | 23 | $0.509 \pm 0.109$ | $0.109 \pm 0.145$ | $0.101 \pm 0.103$ |
| $1296 \le M \le 1316$ | No cut | 19 | $0.222 \pm 0.161$ | $0.581 \pm 0.167$ | $-0.012 \pm 0.092$ |
| $1316 \le M \le 1336$ | No cut | 16 | $0.444 \pm 0.110$ | $0.297 \pm 0.140$ | $0.062 \pm 0.185$ |
| $1336 \le M \le 1356$ | No cut | 11 | $0.455 \pm 0.252$ | $-0.060 \pm 0.194$ | $0.144 \pm 0.130$ |
| $1356 \le M \le 1376$ | No cut | 11 | $0.617 \pm 0.254$ | $-0.182 \pm 0.207$ | $0.655 \pm 0.224$ |
| Stodolsky-Sakurai model | | | 0.373 | 0.216 | 0 |

ified successes the function was generalized to include any number of particles. In its generalized form, the function had several properties not found in the four-point version, the most important of which are multiperipherality and resonance production. Since the $N$-point function serves as a prototype for much theoretical effort, it became evident that its properties should be tested against experiment to establish their validity. The early fits of the five-point function by Peterson,[5] Tornqvist,[6] CRTT,[7] and others showed that the function did seem to fit the data rather well. The work of CRTT showed that the function could simultaneously fit crossed reactions as well, something other models could not easily do. In our review of these early works, we found that much of the global success of the fits seemed to reflect a judicious input into the model and not a direct consequence of the model itself. Therefore, in an earlier work,[10] we undertook a study of the

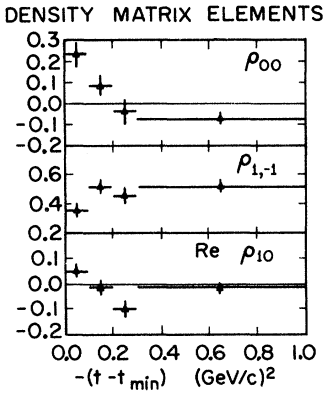


FIG. 18. Density matrix elements of the $K^*(890)$ as a function of the invariant four-momentum transfer from the beam.

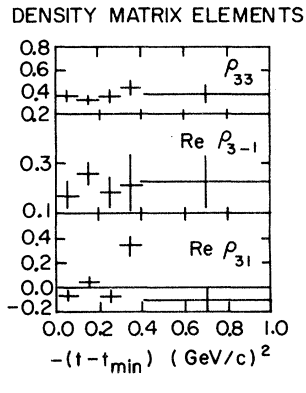


FIG. 19. Density matrix elements of the Δ(1236) as a function of the invariant four-momentum transfer from the target.

five-point model to determine its predictive capacity and isolate the effects of the input. We were fortunate to have on hand some of the data described in this paper. Since this reaction is also one of the ones studied by CRTT, we found that we should make a thorough study of the effects of input. We found that without narrowing the accepted width of the $\Delta(1236)$, we could not obtain a reasonable fit to the data with the model of CRTT. We did conclude that the problem with the model of CRTT was the use of a kinematic factor which pinched the edges of phase space, preventing the resonances from peaking up. In our work we proposed a simple modification of CRTT's model that did away with the pinching, thereby permitting the five-point function to display itself.

In this work we review some of the considerations of our model and extend its test to other energies. In subsection B below we discuss the importance of this particular reaction and the data which we will fit. Subsections C–G discuss the formulation of our model; in subsection H we discuss the method used in the Monte Carlo calculations; in subsection I, the results of our fits; and in subsection J, our conclusions.

### B. Importance of This Reaction

As will be discussed in subsection C, the five-point model uses, in general, twelve separate amplitudes. This requirement presents a large computational task, especially if there are channels in the reaction where there are known to be several dominant trajectories exchanged. Since in principle all trajectories would have to be included in every possible combination, the result would be many amplitudes and a prohibitive computational requirement. The virtue in our reaction is that there are several exotic channels, thereby permitting us to eliminate many of the diagrams. In addition, only a few of the possible channels have more than one dominant trajectory, so we save greatly on the number of additional amplitudes.

The role of the Pomeranchon trajectory in purely dual models is not certain, but it is believed that it has no place in a resonance model such as ours. Hence, it is advisable to choose reactions where the Pomeron does not couple so that its effect need not be of concern. There is some evidence to support the assumption that the Pomeranchon does not couple to our reaction. The Pomeranchon is forbidden at the $K^+\overline{K}^0$ vertex by isospin conservation, and since the $K^*$ cross sections decrease rapidly with energy, we are reasonably certain that the Pomeranchon is not present in the $p\bar{p}$ channel.[19,20]

An additional important point is that our data are at a high energy with excellent statistics free from contamination. Our energy, 4.8 GeV in the center-of-mass system, is reasonably close to to the high-energy range where multiperipheral effects are important, and at the same time, it is close to the resonance-energy regions. Although we concern ourselves with only one model in this paper, it is clear that our data can give any model a rigorous and detailed test.

The data used in this paper come from two sources. The 12-GeV/$c$ data have been described earlier in this paper. The 9- and 4.6-GeV/$c$ data come to us, courtesy of A. Firestone of the Trilling-Goldhaber Group at the Lawrence Berkeley Laboratory and have been discussed in detail elsewhere.[21,22]

### C. Formulation of the Model

The Veneziano model does not properly treat processes involving fermions. Careful analysis of the resonance spectrum predicted by the model

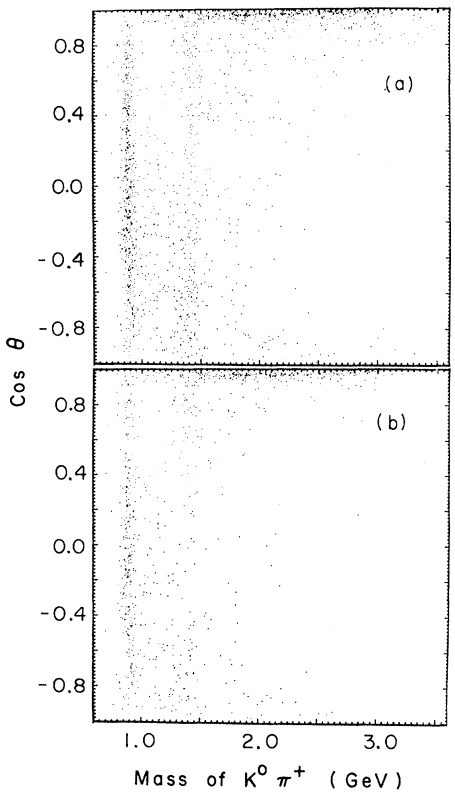


FIG. 20. (a) A scatter plot of $K^0\pi^+$ mass versus cos $\theta$ in the Jackson frame. (b) A similar plot except that a cut of $-t' < 0.2$ on the momentum transfer to the $K^0\pi^+$ mass from the beam was imposed. The statistics are too poor to support the hypothesis of a resonance at 1.85 GeV.

TABLE VI. Phenomenological trajectory functions of the form $\alpha(s) = a + bs + ic(s - s_1)\,\theta(s - s_2)$, where $a$, $b$, $c$, $s_1$, and $s_2$ are obtained by interpolating from data found in the Particle Data Group[23] compilation. The fits were done with pen and ruler, and the number of significant figures presented should not be taken as indicative of the errors.

| Trajectory | |
|---|---|
| $\rho - A_2$ | $\alpha_\rho(s) = 0.477 + 0.894s + 0.0194i(s + 3.79)\theta(s - 0.080)$ |
| $\omega - f$ | $\alpha_\omega = 0.377 + 1.014s + 0.186i(s - 0.56)\theta(s - 0.171)$ |
| $K^* - K^{**}$ | $\alpha_{K^*}(s) = 0.331 + 0.841s + 0.064i(s - 0.203)\theta(s - 0.401)$ |
| $\pi$ | $\alpha_\pi(s) = 0.9(s - 0.019)$ |
| $\Delta$ | $\alpha_\Delta(s) = 0.152 + 0.881s + 0.125i(s - 0.46)\theta(s - 1.15)$ |
| $Y_1^*$ | $\alpha_{Y_1^*}(s) = -0.265 + 0.92s + 0.096i(s - 1.43)\theta(s - 1.56)$ |
| $N_\alpha$ | $\alpha_N(s) = -0.400 + 1.02s + 0.125i(s - 0.893)\theta(s - 1.15)$ |
| $\Lambda$ | $\alpha_\Lambda(s) = -0.674 + 0.943s + 0.07i(s - 1.24)\theta(s - 1.75)$ |

reveals unwanted parity doublets and ghosts. So far, methods suggested to remove these problems have not proved fruitful. Ignoring spin-related theoretical problems limits the validity of this approach.

To remove poles from the real axis, we insert phenomenological trajectory functions directly into the argument of the five-point function $B_5$ and ignore the problem of ancestor poles. Above threshold, the imaginary part of the trajectory function is chosen to be an interpolation of the formula

$$\mathrm{Im}\alpha(s)\big|_{s=s_{\mathrm{res}}} = \frac{d(\mathrm{Re}\alpha(s))}{ds}\bigg|_{s=s_{\mathrm{res}}} M_{\mathrm{res}}\Gamma_{\mathrm{res}}\,, \qquad (6)$$

valid at the resonance poles. Below threshold, the trajectory is kept real. In all instances encountered in this study, a linear interpolation of Im$\alpha$ was used. The parametrization of the Regge trajectories used is shown in Table VI. The data used to determine the parameters for the trajectories were obtained from the latest compilation by the Particle Data Group.[23] Among the minor differences between our trajectories and those used by CRTT is that for Re$\alpha(s)$ we use the same slope above and below threshold instead of using a universal slope of 0.9 GeV$^{-2}$ below threshold.

We assume that we can write the matrix element in the form

$$M = \sum_{j=1}^{N}\sum_{i=1}^{12} K_{ji}B_5(\alpha_i)\,, \qquad (7)$$

where the index $i$ runs over the twelve distinct orderings of the five external particles not related by cyclic or anticyclic permutations. The function $B_5$ is a Bardakci-Ruegg five-point function with arguments related to the trajectory functions of the graphs for the $i$th ordering.[1,3] The factor $K_{ij}$ is an invariant kinematic factor, and the index $j$ labels the different types of external kinematic factors employed. We do not consider terms of nonleading order (satellites), so we require that each term have the correct Regge behavior and the proper angular momentum for the leading resonance in each channel.

If we assume the absence of exotic resonances, then we can neglect all ordering which have exotic channels. This leaves only the four diagrams shown in Fig. 21. If we further assume the relevance of the Harari-Rosner quark rules,[24,14] we can eliminate Fig. 21(d) which corresponds to the nonplanar quark graph. The elimination of this graph ensures strong exchange degeneracy between the $K^*(890)$ and $K^*(1420)$ trajectories.[25]

The primary input into the model is the trajectory in each channel. In a channel where there is more than one possible exchange, we either make a choice based upon intercepts and couplings or we allow terms with each possible combination of

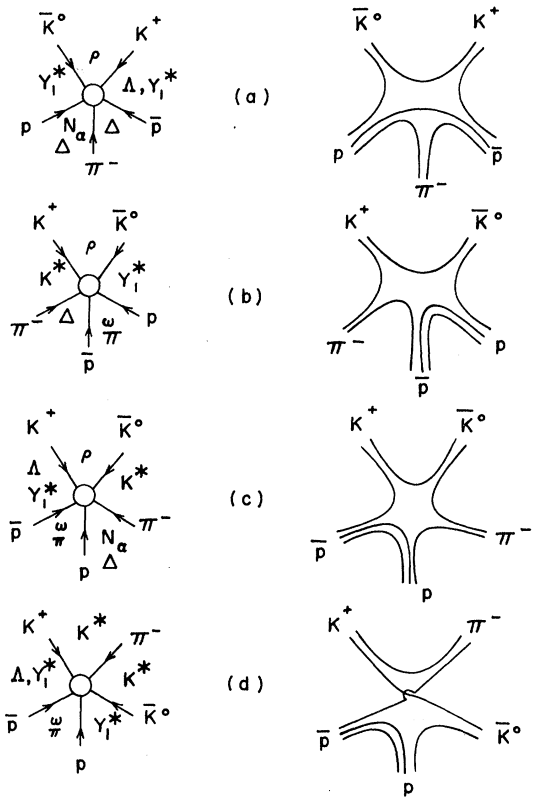


FIG. 21. This shows the four orderings of the external particles which do not produce exotic channels and gives the trajectories which can contribute to the amplitude. At the right of each graph is the Harari-Rosner quark diagram corresponding to it. For graph (d), the quark diagram is nonplanar and by the Harari-Rosner rules should not contribute. Since graphs (c) and (d) differ only by the interchange (3) $\leftrightarrow$ (5) in the $K^*$ channel, the omission of graph (d) ensures strong exchange degeneracy between $K^*(890)$ and $K^*(1420)$.

the trajectories. In the $pK^-$ channel we have to choose between the exchange-degenerate $I=0\Lambda_\alpha - \Lambda_\beta$ trajectory, which includes the $\Lambda$ and the $\Lambda(1520, J^P=\frac{3}{2}^-)$, and the exchange-degenerate $Y_1^*$ trajectory, containing the $Y^*(1385, J^P=\frac{3}{2}^+)$ and the $Y^*(1765, J^P=\frac{5}{2}^-)$. In the $p\pi^-$ channel we have a choice between the $I=\frac{1}{2}$ exchange-degenerate $N_\alpha - N_\gamma$, which includes the nucleon and the $N^*(1520, J^P=\frac{3}{2}^-)$, and the exchange-degenerate $\Delta - N_\beta$, which includes the $I=\frac{3}{2}$ $\Delta(1236, J^P=\frac{3}{2}^+)$ and the $I=\frac{1}{2}$ $N^*(1670, J^P=\frac{5}{2}^-)$. CRTT made the choice $\Lambda_\alpha - \Lambda_\beta$ and $N_\alpha$. They were supported in this by the results of Bartsch *et al.*,[8] who investigated these options in the reaction $K^-p \to \overline{K}^0\pi^-p$ under the limitation of one trajectory per channel. In one variation of our model we permit both $N_\alpha$ and $\Delta$ in the $p\pi^-$ channel. In the $p\bar{p}$ channel the possibilities include the $\omega, \rho$ and the $\pi$. Both CRTT and Bartsch *et al.* used vector exchange in the $p\bar{p}$ channel, although they mentioned the possibility that their discrepancies were due to $\pi$ exchange. Fits to the density matrix of our reaction in the $K^*(890)$ mass region show that for $0 < -t < 0.05$ (GeV/$c$)$^2$, the ratio of pseudoscalar exchange to vector exchange is large, so we also included pion exchange in some versions of our model. Of the vector exchanges, we chose the $\omega$ over the $\rho$, since the experimental evidence for $K^*$ production favors the $\omega$ exchange.[26]

The normalization of each $B_5$ term in the sum is not intrinsically determined, although signature arguments can be used to fix ratios. The requirement of a definite signature $\Delta$ in the $p\pi^+$ channel fixes the ratio of the constants in front of Figs. 21(a) and 21(b) to be 1:1. A definite signature $N_\alpha$ trajectory [eliminating the $N^*(1520)$] in the $p\pi^-$ channel implies the ratio of the coefficients of Figs. 21(a) and 21 (c) to be 1:1. Again $K^*$ exchange degeneracy requires that Fig. 21(d) be neglected.

### D. Kinematic Factors

The first pole in the argument of $B_5(-\alpha_{12}, -\alpha_{23}, -\alpha_{34}, -\alpha_{45}, \alpha_{51})$ occurs at $\alpha=0$ in each channel and corresponds to a spin-0 resonance. In order to incorporate fermions and trajectories with their first resonance at $l=1$, it is convenient to shift the argument of the five-point function and to use the kinematic factor $K_{ij}$ to ensure the proper asymptotic behavior and angular momentum structure for the amplitude.

### E. Vector Exchange

One possible form of the kinematic factor was discussed by Tornqvist[6] under the assumption of dominance of vector exchange in the $p\bar{p}$ channel. For reference, let us number the particles in the order $K^+p \to \pi^+pK^0$ and let $p^1+p^2 \to p^3+p^4+p^5$ be the corresponding four-momenta. The most general axial vector formed from the three momenta is

$$A_\mu = \epsilon_{\mu\nu\rho\sigma} p_1^\nu p_3^\rho p_5^\sigma . \tag{8}$$

We then consider the kinematic factor

$$K_{ii} = \bar{U}(p_4)(A_\mu p_2^\mu + C_1 A_\nu \gamma_\nu) U(p_2) \tag{9}$$

to be the same for each orientation $i$. The spin-averaged differential cross section would then have terms proportional to

$$|M|^2 \propto \left| \sum_i B_5(\alpha_i) \right|^2 \{[(M_2+M_4)^2 - t_{24}]E^2 + 2C_1(M_2+M_4)E^2 + 2C_1^2E^2 + C_1^2[t_{24} - (M_2-M_4)^2]A\cdot A\}, \tag{10}$$

where

$$E = p_2 A = + \epsilon_{\mu\nu\rho\sigma} p_1^\mu p_2^\nu p_3^\rho p_4^\sigma , \tag{11}$$

and $M_2$ and $M_4$ are the fermion masses, and $t_{24} = -(p_2-p_4)^2$. In this case we have equal fermion masses, so that $M_2 - M_4 = 0$. The factor $K_{ij}$ ensures the correct asymptotic behavior of the amplitude if the argument of the $B_5$ function is $(1-\alpha)$ in the boson channel and $(\frac{3}{2}-\alpha)$ in the fermion channels. In this reaction, however, the $N_\alpha$ and the $\Lambda$ have their first poles at $J=\frac{1}{2}$, and we have to be careful about the exchange of these trajectories. Tornqvist[6] points out that since $t_{24}$ is small in the physical region, it is not a bad approximation to replace the entire multiplier of the $B_5$ function with

$$\approx C_2 E^2 . \tag{12}$$

The form of the complete amplitude used by CRTT is then

$$M = E[B_5(\tfrac{1}{2}-N_{23}, \tfrac{3}{2}-\Delta_{34}, \tfrac{1}{2}-\Lambda_{41}, 1-\rho_{15}, \tfrac{3}{2}-Y_{52}^*) + B_5(1-\rho_{24}, \tfrac{3}{2}-Y_{25}^*, 1-\rho_{51}, 1-K_{13}^*, \tfrac{3}{2}-\Lambda_{34}) + B_5(1-\rho_{24}, \tfrac{1}{2}-N_{23}, 1-K_{35}^*, 1-\rho_{51}, \tfrac{1}{2}-\Lambda_{14})], \tag{13}$$

where $X_{ij}$ is shorthand for the trajectory function $\alpha_X[(p_i \pm p_j)^2]$. To save space we abbreviate the three terms in the above expression by $B_5(A)$, $B_5(B)$, $B_5(C)$, respectively. It should be noted that as it is written, the above expression does not have correct asymptotic behavior when fermion trajectories are exchanged. To get the correct asymptotic behavior, CRTT made the additional modification of

$$\tfrac{1}{2} - N_{23} \to 1 - N_{23},$$
$$\tfrac{1}{2} - \Lambda_{41} \to 1 - \Lambda_{41}, \qquad (14)$$
$$\tfrac{3}{2} - Y^*_{52} \to 1 - Y^*_{52}.$$

Since the problem of spin has not been solved within the context of the Veneziano model, it is probably unwise to be too dogmatic about the form of the kinematic factor. If we allow axial-vector exchange in the $p\bar{p}$ channel, we can consider a factor such as

$$K_{2i} = Q^\mu \bar{U}(p_4)(i\gamma_5 p_\mu + C_3\gamma_5\gamma_\mu)U(p_2), \qquad (15)$$

where $Q^\mu$ is a vector formed from the meson momenta. Within the spirit of the approximations that led to our amplitude, it is consistent to use a kinematic factor which is a linear polynomial in the various channel-invariants. We therefore consider terms such as

$$M_2 = (S_{23}+S_{34}+S_{41}+S_{15}+S_{52})B_5(A) + (S_{42}+S_{25}+S_{51}+S_{13}+S_{34})B_5(B) + (S_{42}+S_{23}+S_{35}+S_{51}+S_{14})B_5(C), \qquad (16)$$

which have the advantage of simplicity but the disadvantage of treating all channels, both bosons and fermions equally, as well as introducing a mixture of $l=0$ with the $l=1$ in the residue of the first pole in each channel. Again, to make the asymptotic behavior of this second amplitude correct, it is convenient to use $(1-\alpha)$ as the argument of a fermion trajectory below threshold.

### F. Pion Exchange

Since the fits to the density matrix elements of the $K^*(890)$ as a function of energy show an appreciable contribution from pseudoscalar exchange in the $p\bar{p}$ channel, we anticipate the need for pion exchange in our fits. Rough consistency with the Lovelace-Shapiro-Yellin[27] formula for the scattering of four pseudoscalars suggests we include in our amplitude a term such as

$$(-\rho_{15} - \Lambda_{14})B_5(A) + (1 - \rho_{15} - K^*_{13})B_5(B) + (1 - \rho_{15} - K^*_{35})B_5(C). \qquad (17)$$

In the $B_5$ functions the pion trajectory replaces the $\rho$ trajectory in the $p\bar{p}$ channel. That is, the argument $(1-\rho_{24})$ is now replaced by $(-\pi_{24})$. Since $B_5(A)$ does not have a $p\bar{p}$ channel, the first term is included to ensure the approximate maintenance of proper signature of the $\Delta^{++}$ trajectory in the $p\pi^+$ channel. This signature property is obtained between the first and second terms in the above expression if we have equality among the trajectory intercepts with

TABLE VII. Versions of the model.

| Version | Matrix element |
|---|---|
| 1 | $\lvert V(A)+V(B)+V(C)\rvert^2$ |
| 2 | $\lvert V(A)+V(B)+V(C)\rvert^2 + C_1\lvert W(A)+W(B)+W(C)\rvert^2 + C_2\lvert \pi(A)+\pi(B)+\pi(C)\rvert^2$ |
| 3 | $\lvert (V(A)+V(B)+V(C)) + C_1(W(A)+W(B)+W(C)) + C_2(\pi(A)+\pi(B)+\pi(C))\rvert^2$ |
| 4 | $\lvert (V(A)+V(B)+V(C)) + C_1(W(A)+W(B)+W(C)) + (C_2+iC_3)(\pi(A)+\pi(B)+\pi(C))\rvert^2$ |
| 5 | $\lvert (V(A)+V(B)) + C_1V(C) + C_2(W(A)+W(B)) + C_3W(C) + C_4(\pi(A)+\pi(B)) + C_5\pi(C)\rvert^2$ |
| 6 | $\lvert V(A)+V(B)+C_1V(C)\rvert^2 + \lvert C_2(W(A)+W(B)) + C_3W(C)\rvert^2 + \lvert C_4(\pi(A)+\pi(B)) + C_5\pi(C)\rvert^2$ |
| 7 | same as 5 but replace $N_\alpha$ by $\Delta$ in $p\pi^-$ channel |
| 8 | $\lvert C_1(V(A)+V(B)) + V(C) + C_2(W(A)+W(B)) + C_3W(C)\rvert^2 + \lvert C_4(\pi(A)+\pi(B)) + C_5\pi(C)\rvert^2$ |

$$\alpha_{K^*}(0) - 1 = \alpha_\Lambda(0). \qquad (18)$$

The approximate values inserted from Table I yield

$$-0.7 \approx -0.7, \qquad (19)$$

showing that the equality is approximately satisfied.

### G. Listing of Our Models

Although in this paper we concern ourselves only with one version of the model, version 8, we present a short description of the other versions that we have studied in our previous work. The first version of the model listed in Table VII is similar to that of CRTT. It uses only vector-meson exchange in the $p\bar{p}$ channel and the approximate kinematic factor $CE$. We also attempted to use the full form of the kinematic factor with $C_1$ as an arbitrary constant and without shifting the fermion trajectories below threshold, but this did not achieve an improvement over the approximate form $CE$ with trajectories shifted. The main problem of both these versions was in the region of the $\Delta(1236)$ resonance, which is very prominent in our data and nearly dominates the $p\pi^+$ mass distribution. Because the $\Delta(1236)$ region is quite near the edge of phase space where the kinematic factors are small, these forms of the model gave too few events in the $\Delta$ peak and too many events in the recurrences. This problem could be partially circumvented by narrowing the width of the $\Delta$ from the commonly accepted value of 120 MeV to 70 MeV in order to raise the height of the $\Delta$ peak. Of course, this does not solve the problem of having too few $\Delta$ events and too many events in the high $p\pi^+$ mass regions. In the data, some one-third of the events are in the $\Delta$ peak, so that under-

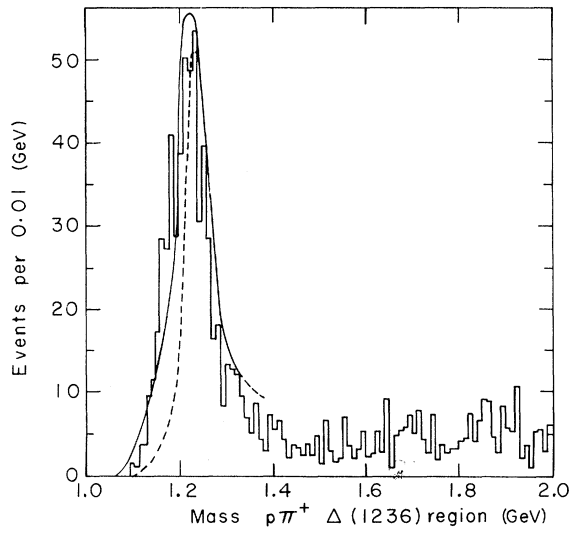


FIG. 22. Data in the Δ(1236) region. The solid curve is the prediction of the $W$ terms using a Δ-trajectory with $\Gamma_{\Delta(1236)}$= 120 MeV. The dotted curve is the prediction of the $V$ terms using a width of 80 MeV. Normalization of the curves is done to the peak of the data.

estimating this peak by a factor of 2 represents a serious discrepancy, which gets worse with increasing energy. The $M_2$ matrix element, because of its polynomial kinematic factor, avoids much of this problem (see Fig. 22).

In order to distinguish between the various versions of the model, we include the listing in Table VII. Here $V(A)$, $V(B)$, $V(C)$ are the three terms in the $M_1$ matrix element; $W(A)$, $W(B)$, and $W(C)$ refer to the three terms of $M_2$; and $\pi(A)$, $\pi(B)$, and $\pi(C)$ refer to the three pion terms. In versions 1–4 we maintained definite signature $N_\alpha$ trajectory in the $p\pi^-$ channel by keeping the ratio of Figs. 21(a)–21(c) as 1:1. Since the $N^*(1520)$ can couple to this channel as well as the nucleon [not to mention the Δ(1236) and the $N^*(1670)$], it is probably not reasonable to require definite signature. In versions 5–8 we break signature in this channel by allowing Fig. 21(c) to have a different coefficient from Fig. 21(a). In version 7 we investigated the possibility of using the $\Delta - N_\beta$ combinations in the $p\pi^-$ channel as well as the $N_\alpha - N_\gamma$. As shown in Table VII we include versions in which terms of different types are added either coherently or incoherently, depending on the detailed structure assumed. In Table VIII the values of the constants of Table VII are determined by a maximum-likelihood fitted program. These tables are only for the 12-GeV/$c$ data. Of these various versions, version 8 had the most success at 12 GeV/$c$, so we devote the remainder of this paper to a test of this version at lower energies.

TABLE VIII. Results of fits.

| Version | $C_1$ | $C_2$ | $C_3$ | $C_4$ | $C_5$ |
|---|---|---|---|---|---|
| 1 | ... | ... | ... | ... | ... |
| 2 | $2.04\times10^{-3}\pm1.2\times10^{-4}$ | $2.48\times10^{-4}\pm5.2\times10^{-5}$ | ... | ... | ... |
| 3 | $-2.39\times10^{-3}\pm2.6\times10^{-3}$ | $-1.67\times10^{-2}\pm1.7\times10^{-3}$ | ... | ... | ... |
| 4 | $1.29\times10^{-3}\pm1.4\times10^{-3}$ | $-2.94\times10^{-3}\pm3.7\times10^{-3}$ | $2.39\times10^{-2}\pm1.2\times10^{-3}$ | ... | ... |
| 5 | $-6.30\times10^{-2}\pm1.8\times10^{-2}$ | $-1.89\times10^{-2}\pm1.2\times10^{-3}$ | $4.8\times10^{-3}\pm1.2\times10^{-3}$ | $-1.54\times10^{-3}\pm2.3\times10^{-3}$ | $-5.95\times10^{-3}\pm1.1\times10^{-3}$ |
| 6 | $3.60\times10^{-1}\pm6.0\times10^{-2}$ | $1.16\times10^{-2}\pm1.6\times10^{-3}$ | $1.97\times10^{-3}\pm1.3\times10^{-3}$ | $2.75\times10^{-2}\pm1.62\times10^{-3}$ | $-5.17\times10^{-4}\pm1.4\times10^{-3}$ |
| 7 | $-9.13\times10^{-2}\pm3\times10^{-2}$ | $-2.43\times10^{-2}\pm1\times10^{-3}$ | $3.61\times10^{-3}\pm1\times10^{-3}$ | $-1.65\times10^{-2}\pm1.7\times10^{-3}$ | $-4.21\times10^{-3}\pm1.2\times10^{-3}$ |
| 8 | $-3.71\times10^{-2}\pm0.02$ | $-1.64\times10^{-2}\pm8\times10^{-4}$ | $8.99\times10^{-4}\pm9\times10^{-4}$ | $2.02\times10^{-2}\pm1\times10^{-3}$ | $4.88\times10^{-3}\pm8\times10^{-4}$ |

### H. Computational Procedures

#### 1. *Monte Carlo*

All computations were done on the Lawrence Berkeley Laboratory's CDC 6600 computers. The computations were in two parts. First, we employed Monte Carlo procedures to do the evaluation of the matrix element in multidimensional phase space. Second, we employed maximum-likelihood procedures to do the fits to the data. Below we briefly describe the procedures and the programs used.

The program KAON performed the Monte Carlo integration and evaluation of the five-point function. This program consisted of three parts: (1) the generation of Monte Carlo events, (2) evaluation of the five-point function, and (3) the plotting of the various distributions of interest. The heart of the Monte Carlo generation consisted of the subroutine SAGE.[28] The efficiency of the Monte Carlo generation depends very much on the structure of the matrix element. For simple matrix elements generation of events in uniform phase space may suffice; however, for complicated matrix elements uniform generation is often inefficient. SAGE has the following important options: (1) generation of events with uniform density in Lorentz-invariant phase space, (2) generation of events with Breit-Wigner density distributions, (3) generation of events with $e^{at}$ and $1/(t-a^2)^2$ four-momentum transfer squared distributions, and (4) general decay angular distributions. There are several other options which were not used and, consequently, will not be discussed. Through trial and error, we found that we needed to employ all of the above options of SAGE in order to make our calculations economically feasible. At 12 GeV/$c$, generating events uniformly in phase space gave us an efficiency[29] on the order of 0.1%. By employing the SAGE options, we were able to increase the efficiency to 16%.

We used the following general phase-space density distribution:

$$g(\phi) = \sum_{i=1}^{M} N_i\, g_i(\phi)/G_i\,, \tag{20}$$

where $N_i$ is the number of events generated with density destribution $g_i(\phi)$ and $M$ is the number of distributions. $\phi$ represents the phase space variables. $G_i$ is given by

$$G_i = \int_V g_i(\phi) d^n\phi\,, \tag{21}$$

and is just the average phase-space weight for events generated with frequency $g_i(\phi)$. $V$ is the phase-space volume. The values of $G_i$ must be known in advance and are obtained by doing separate integrations. The weight assigned each event generated with frequency $g_i$ is

$$W(\phi) = |M|^2[w(2)/G_i]/[g(\phi)]\,, \tag{22}$$

where $M$ represents the matrix element.

In order to improve efficiency, it is necessary to match the generation density to the matrix element squared as closely as possible. For the five-point function it was necessary to match all the resonances in the final state. At 12 GeV/$c$, there are some 28 poles in the five-point functions used. Therefore, we generated Breit-Wigner distributions both with $e^{at}$ and $e^{au}$ distributions for each resonance. In addition, we generated events with uniform mass distribution but with an $e^{at}$ distribution for each final-state particle both with respect to the beam and with respect to the target. The various values of $a$ in the exponential distributions were determined for each distribution by doing an approximate Monte Carlo integration of the matrix element and doing eyeball approximations to the momentum transfers. We note that the current version of SAGE has an option by means of which such parameters may be optimized for better efficiency (note that also the number of events generated according to distribution $g_i$ may also be considered a parameter).

The evaluation of the five-point function was done by SPIDER. This routine is based on the algorithm of Hopkinson[30] but with several programming changes. The equations of the algorithm are presented in Part 2.

The various distributions of interest were plotted by KIOWA and NIZRPLT, standard LBL Group A programs.[31]

We wish to emphasize the efficiency of the above procedure by pointing out that of all the computer time used to do the theoretical calculations (at 12 GeV/$c$), it took longer to process and plot the events than to generate them and evaluate the five-point function. In total, it required some 500 CP seconds[32] to generate and process 25 000 events. This time could be reduced by up to an order of magnitude by coding the analysis programs more efficiently and using the full power of SAGE.

#### 2. *The Bardakci-Ruegg $B_5$ Function*

The Bardakci-Ruegg five-point function is a generalization of the Euler Beta function to five variables. It is an analytic function of all of its variables, and was initially defined through its integral representation:

$$B_5(x_1, x_2, x_3, x_4, x_5) = \int_0^1 \int_0^1 du_2 du_4 (1-u_2)^{x_1-1} u_2^{x_2-1} (1-u_2u_4)^{x_3-x_1-x_5} u_4^{x_4-1} (1-u_4)^{x_5-1}. \quad (23)$$

A computationally useful series representation may be obtained from the above expression by expanding the factor $(1-u_2u_4)^{x_3-x_5-x_1}$ by the binomial theorem. This series will be convergent throughout the region of integration and will have the general term

$$-\binom{-z_3}{n}(u_2u_4)^n, \quad (24)$$

where $z_3 = x_1 - x_3 + x_5$. This series expansion separates the integral into two integrals, each of which may be done separately. In fact, the remaining integrals are just the Euler beta functions:

$$\int_0^1 du\,(1-u)^{a-1}u^{b-1} = B_4(a,b) \equiv \frac{\Gamma(a)\Gamma(b)}{\Gamma(a+b)}. \quad (25)$$

The series thus becomes

$$B_5 = \sum_{k=0}^{\infty} (-1)^k \binom{-z_3}{k} \frac{\Gamma(x_1)\Gamma(x_2+k)\Gamma(x_4+k)\Gamma(x_5)}{\Gamma(x_1+x_2+k)\Gamma(x_4+x_5+k)}. \quad (26)$$

The series part of the above expression is just the usual hypergeometric series with unit argument

$${}_3F_2(x_2, z_3, x_4; x_1+x_2, x_4+x_5; 1), \quad (27)$$

which converges when

$$\mathrm{Re}[1+(x_1+x_2)+(x_4+x_5)-x_2-z_3-x_4)] > 1, \quad (28)$$

that is, when $\mathrm{Re}(x_3)$ is positive.

The series representation of the $B_5$ function forms the basis of the computational method used in our program. Further details and recursion relations between contiguous $B_5$ functions may be found in Hopkinson.[30]

### I. Discussion of Results

In Figs. 3–17 we present the comparison of the predictions of the generalized Veneziano model with data at three energies. We do this comparison only for version 8 of the model since it was the best at 12 GeV/$c$ and since space limitations forbid the presentation of other versions. In version 8 of the model there are five adjustable parameters, neglecting over-all normalization. We do not expect these parameters to be energy-independent, so we have fitted them to the data at each of the energies. Thus, the theoretical predictions represent the best fit to the data at the respective energies. To study the energy dependence of the parameters, we have plotted them as a function of the beam momenta in Fig. 23. As may be seen, parameters 1 and 3 are, to within less than one standard deviation, independent of energy, although 3 exhibits a trend of increasing with decreasing energy. Parameters 4 and 5 are slowly varying with energy. Parameter 1 represents the amount of signature breaking in the $p\pi^-$ channel for the $V$ terms of the model. The fact that parameter 1 does not change appreciably with energy implies that for the $V$ terms the signature breaking varies slowly with energy. Parameters 2 and 3 represent signature breaking in the same channel for the $W$ terms. Again, the slow variation of these parameters implies that the signature breaking is energy-independent. Another fact to note is that the ratio of parameter 2 to 3 varies slowly with energy. This ratio scales the signature-breaking parametrization of the $W$ terms relative to $W(C)$, whereas parameter 1 scales the signature breaking of the $V$ terms relative to $V(C)$. In view of this we would expect, assuming that the model has a modicum of truth, the energy behavior of parameter 1 and the ratio of 2 to 3 to be similar. This is borne out in Fig. 23. Similar reasoning may be applied to parameters 4 and 5 in the $\pi$ terms which provide the pseudoscalar contribution to the production of the $K^*$'s. It is known that pseudoscalar exchange drops off with increasing energy and these param-

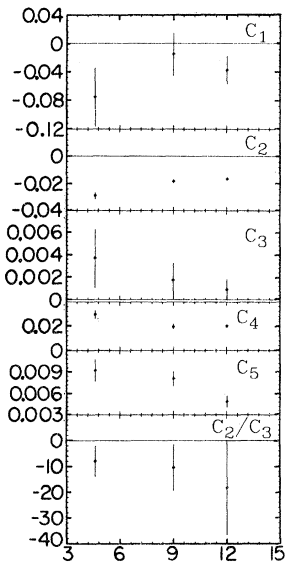


FIG. 23. Fitted parameters of the theory. This plot shows the variation of the five parameters with the beam momentum.

eters display this. However, being energy-dependent, they point out that our model does not handle pseudoscalar exchange properly. This is not too much of a surprise, since the pion trajectory has historically been difficult to handle, especially in dual models.

Figure 3 shows the $K^0\pi^+$ mass spectrum. The fits at 12 and 9 GeV/$c$ are reasonable; however, the fit at 4.6 shows disagreement near 1.7 GeV, a region where there has been a report of a meson.[18] The theory has a pole at this point (the second Regge recurrence of the $K^*$'s) that does not change with energy. The data, on the other hand, do display a small but persistent bump in this region at all energies, but the bump shifts with energy and is, therefore, hard to interpret. We point out that in the 9-GeV/$c$ data, the $K^*(890)$ was found to be too narrow by a standard deviation[22] so the disagreement with theory may be due to a fluctuation in the data.

We note here that when we display the theoretical prediction, we plot the Monte Carlo points directly instead of passing hand drawn curves through them. The reason for this is that errors fluctuate from bin to bin in the plots, often being larger than expected, so a hand-drawn smoothing process can easily be led astray and reflect more the draftsman's optimism than the physics. To this end we

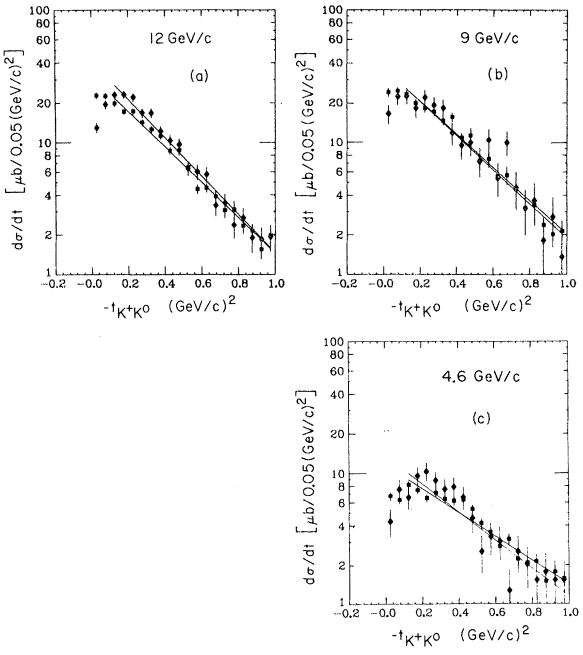


FIG. 24. Exponential fit to the momentum transfer to $K^0$ from the beam. The fits were done to data and theory independently over the interval covered by the displayed lines. The square points are the theory and the diamond points are the data. The fits are excellent.

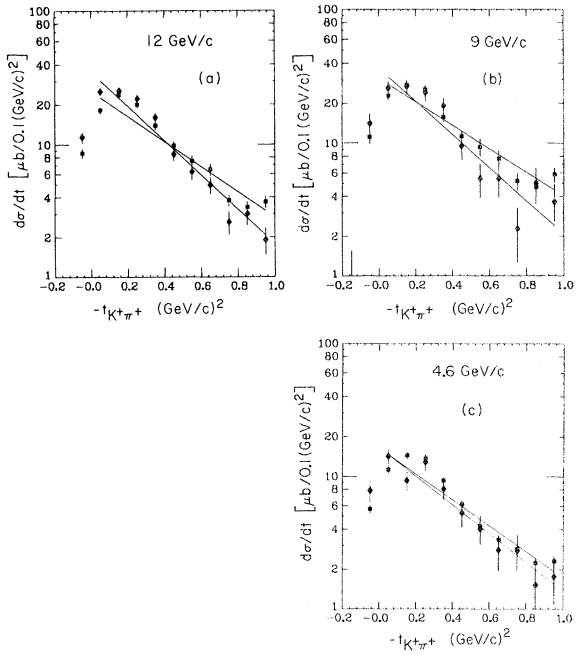


FIG. 25. Exponential fit to the momentum transfer to $\pi^+$ from the beam. Comments for Fig. 24 apply here.

also plot on the same figures the actual Monte Carlo errors (defined as the square root of the sum of the squares of the weights for each bin) to scale in each histogram. The errors in the data can be estimated by merely taking the square root of the contents of a bin. We use only one normalization constant for *all* Figs. 3–17.

Figure 4 shows the $p\pi^+$ mass spectrum. The problem with the $\Delta(1236)$ persists with energy, being worse at 4.6 GeV/$c$. The remaining portion of the mass spectrum is fitted relatively well. In particular, the strong recurrences visible in other formulations of the model do not present serious difficulty.

The $pK^0$ mass spectrum (Fig. 5) fits well at all energies, lending support for the absence of exotic resonances in this channel.

The invariant four-momentum transfer to the $K^0$ (Fig. 6) from the beam fits well at all energies, particularly if one ignores the first few bins. Similarly the four-momentum transfer to the pion relative to the beam (Fig. 7) fits well. The four-momentum transfer to the proton from the target, (Fig. 8) fits exceptionally well, making allowances for the first few bins, and duplicates the narrowing of the distribution with increasing energy. Thus it appears that our model fits the single-particle momentum-transfer distributions well if the particle comes predominantly from an internal vertex of the multiperipheral chain (the pion in our case) and it fits the particles on the extreme ends of the

chain but not in the forward or backward direction. This probably suggests that our kinematic factors are not correct since they shape these distributions in the two directions.

The model underestimates the amount of $K^*(890)$; hence, in the plots of momentum transfer to the $K^*(890)$ the disagreement appears large (Fig. 9). However, if the graphs were renormalized, the disagreement would appear much smaller. In particular, the shape is rather well reproduced away from the leading bins. The peaking in the first bin of the 4.6-GeV/$c$ prediction is due to the large amount of pseudoscalar exchange in this channel. This exchange makes its contribution mostly to the first bin. The sharpness of this contribution comes as no surprise to those who have worked with one-pion exchange models and the absorption models. A similar peaking is also evident in the 9 GeV/$c$ data, although not to the same extent.

The situation is slightly different for the four-momentum transfer to the $K^*(1420)$ (Fig. 12). At 4.6 and 9 GeV/$c$ the data peak in the forward direction, particularly the 9-GeV/$c$ data, so the pion contribution fits nicely. However, at 12 GeV/$c$, the data do not peak, so a discrepancy is evident. The $K^*(1420)$ production must be rather complex since the momentum transfers appear to have strong energy dependence in the forward direction.

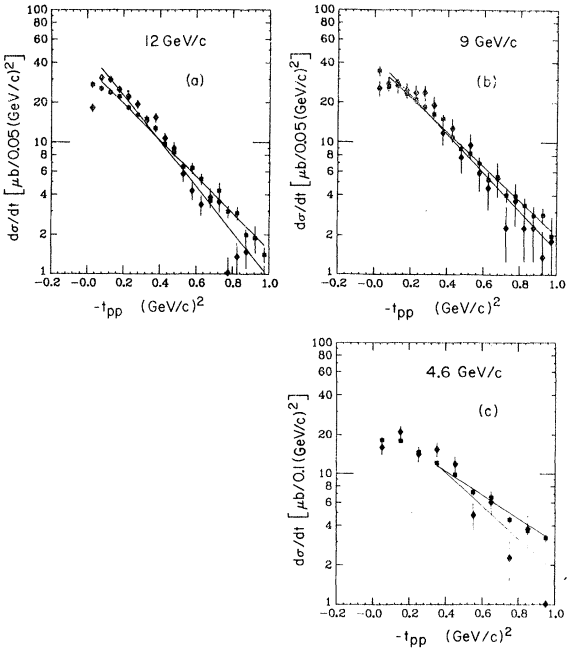


FIG. 26. Exponential fit to the momentum transfer to $p$ from the target. Comments for Fig. 24 apply here.

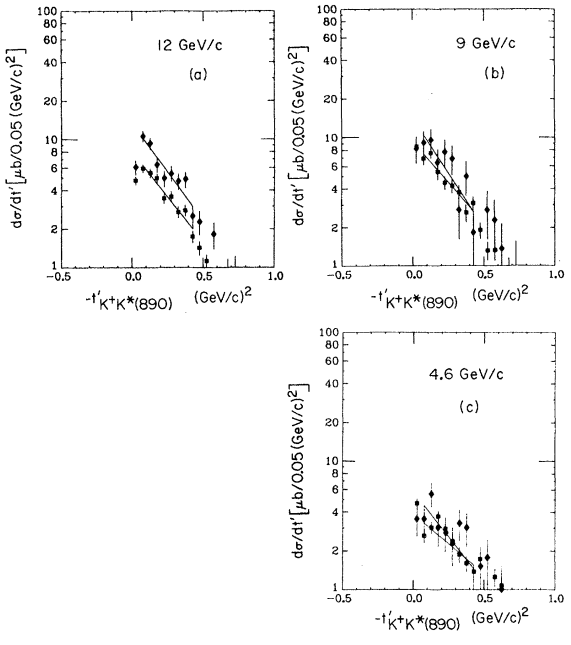


FIG. 27. Exponential fit to the momentum transfer to $K^*(890)$ from the beam. Comments for Fig. 24 apply here.

The momentum transfers to the $\Delta(1236)$ (Fig 15) fail to fit at all energies. This is in large part due to our formulation of the model in which the $\Delta(1236)$ is created by the $W$ terms which do not

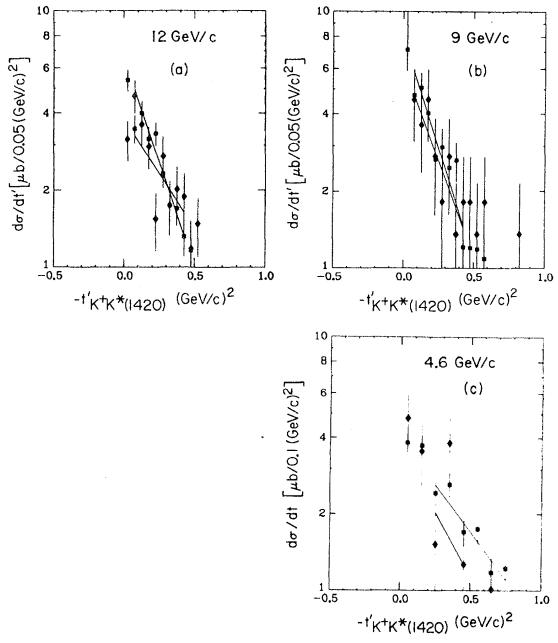


FIG. 28. Exponential fit to the momentum transfer to $K^*(1420)$ from the beam. Comments for Fig. 24 apply here.

TABLE IX. Momentum transfer fits of the form $Be^{At}$, $t$ in units of $(\mathrm{GeV}/c)^2$.

| GeV/$c$ | | $t_{K^+K^0}$ | | $t_{K^+\pi^+}$ | | $t_{p\rho}$ | | $t_{K^+K^*(890)}$ | | $t_{K^+K^*(1420)}$ | | $t_{p\Delta(1236)}$ | |
|---|---|---|---|---|---|---|---|---|---|---|---|---|---|
| | | $B$ | $A$ | $B$ | $A$ | $B$ | $A$ | $B$ | $A$ | $B$ | $A$ | $B$ | $A$ |
| 4.6 | Data | 13.58 | −2.47 | 16.48 | −2.49 | 32.45 | −2.92 | 5.74 | −3.25 | 3.60 | −2.33 | 8.79 | −3.76 |
| | | ±1.50 | ±0.23 | +1.70 | ±0.24 | +3.40 | ±0.19 | +1.30 | ±0.84 | ±1.90 | ±0.87 | ±3.60 | ±1.20 |
| | Theory | 11.67 | −2.10 | 16.36 | −2.25 | 23.89 | −2.08 | 3.88 | −2.16 | 4.00 | −1.72 | 4.68 | −4.82 |
| | | ±0.46 | ±0.08 | +0.61 | ±0.07 | +0.70 | ±0.03 | ±0.35 | ±0.32 | ±0.52 | ±0.23 | ±0.87 | ±0.57 |
| 9 | Data | 36.17 | −2.88 | 36.37 | −2.87 | 43.17 | −3.33 | 13.91 | −3.91 | 6.06 | −3.37 | 31.35 | −7.50 |
| | | ±3.47 | ±0.20 | ±3.44 | ±0.24 | ±3.30 | ±0.19 | ±2.86 | ±0.82 | ±3.20 | ±1.70 | ±9.66 | ±1.10 |
| | Theory | 36.67 | −2.97 | 30.67 | −2.04 | 38.79 | −2.97 | 9.26 | −2.93 | 7.85 | −3.94 | 15.67 | −6.62 |
| | | ±1.68 | ±0.09 | ±1.39 | ±0.10 | ±1.44 | ±0.08 | ±0.93 | ±0.39 | ±1.46 | ±0.64 | ±2.18 | ±0.47 |
| 12 | Data | 40.88 | −3.33 | 35.11 | −2.98 | 48.76 | −3.94 | 13.19 | −3.48 | 3.76 | −1.96 | 43.70 | −7.67 |
| | | ±1.90 | ±0.11 | +1.60 | ±0.11 | ±1.70 | ±0.10 | ±1.40 | ±0.42 | ±1.00 | ±0.90 | ±9.50 | ±0.52 |
| | Theory | 31.52 | −3.08 | 25.15 | −2.18 | 36.46 | −3.17 | 7.94 | −3.25 | 6.46 | −3.71 | 17.80 | −6.72 |
| | | ±1.10 | ±0.07 | ±0.89 | ±0.07 | ±0.95 | ±0.06 | ±0.53 | ±0.26 | ±0.88 | ±0.48 | ±2.30 | ±0.30 |

exhibit the spin-flip character and, consequently, peak in the forward direction.

In Figs. 24–29 we plot the logarithm of the differential cross section versus the momentum transfer to the single particles and the resonances at the various energies. We have fitted these distributions to expressions of the form

$$d\sigma/dt = Be^{at}.$$

The fits were done only for small values of $|t|$.

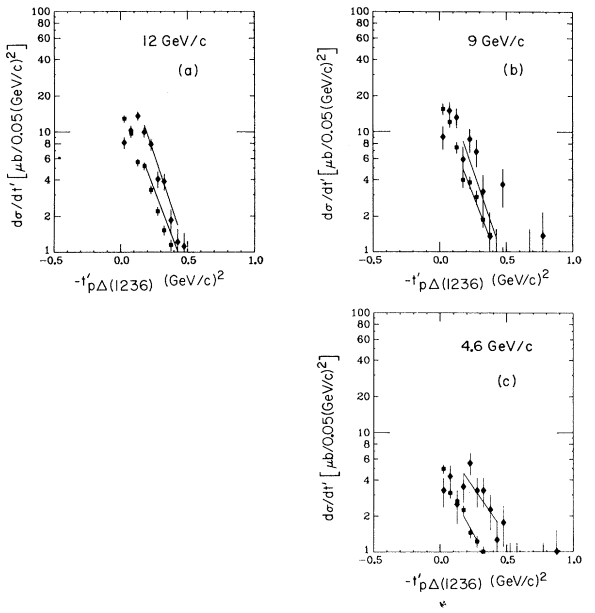


FIG. 29. Exponential fit to the momentum transfer to Δ(1236) from the target. Although the theory does not fit the data in the forward direction, the slopes of the theory and data are quite similar away from the forward direction. Comments for Fig. 24 apply here.

In addition, we ignored the first few bins since it is evident that such a simple parametrization would not apply in these regions. We fitted both the data and the theory. Table IX gives the fitted values of $a$ and $B$ of the above expression. The

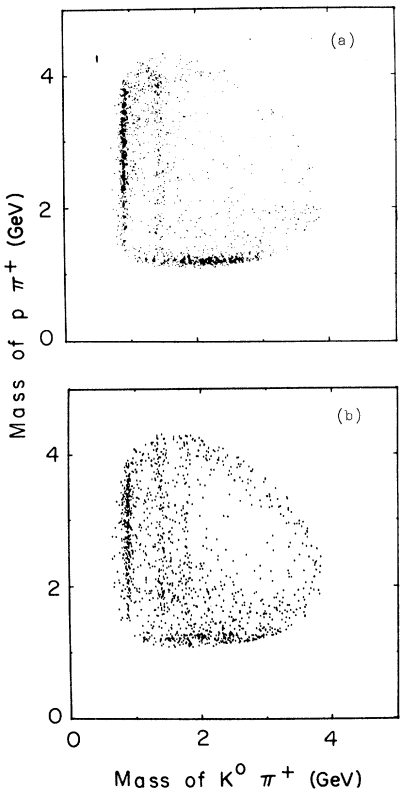


FIG. 30. (a) 12-GeV/$c$ scatter plot of the mass of $K^0\pi^+$ vs $p\pi^+$ for the data. (b) Is a similar plot for the theory. Units are in GeV.

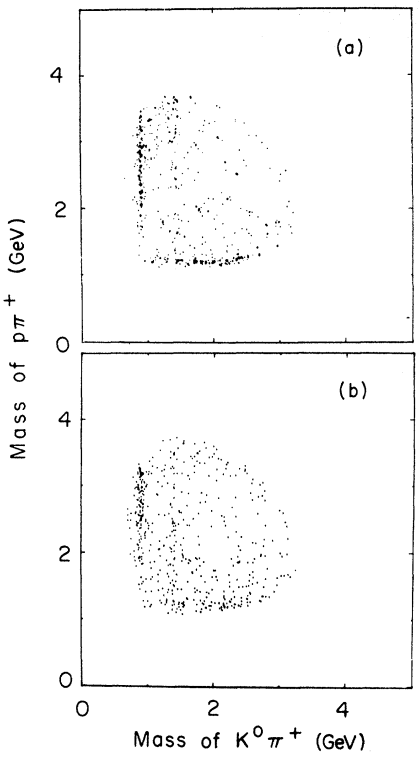


FIG. 31. (a) 9-GeV/$c$ scatter plot of data and (b) of theory for $K^0\pi^+$ vs $p\pi^+$.

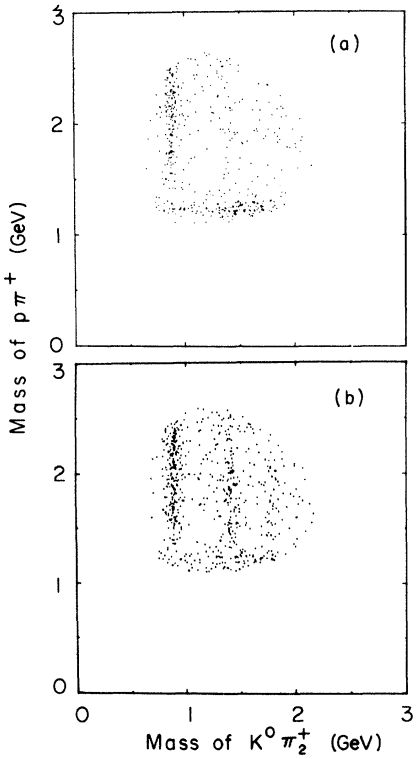


FIG. 32. (a) 4.6-GeV/$c$ scatter plot of data and (b) of theory for $K^0\pi^+$ vs $p\pi^+$.

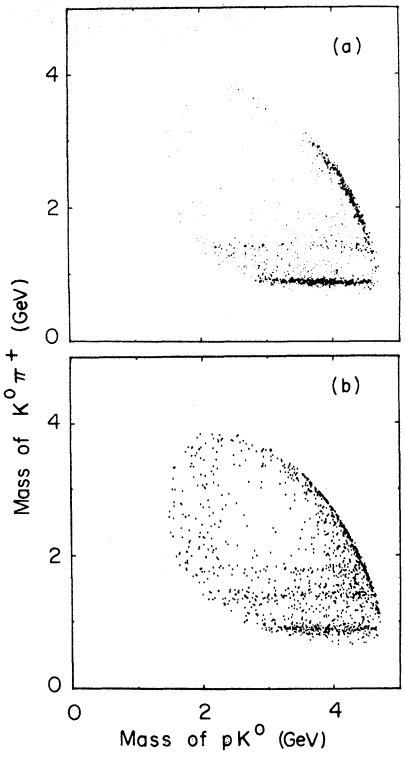


FIG. 33. (a) 12-GeV/$c$ scatter plot of data and (b) of theory for $pK^0$ vs $K^0\pi^+$.

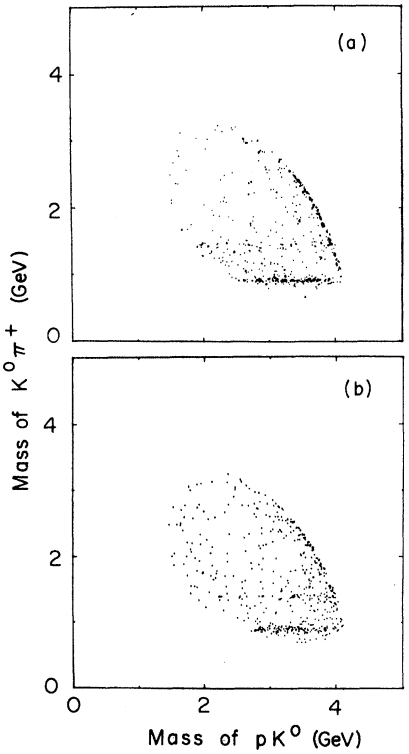


FIG. 34. (a) 9-GeV/$c$ scatter plot of data and (b) of theory for $pK^0$ vs $K^0\pi^+$.

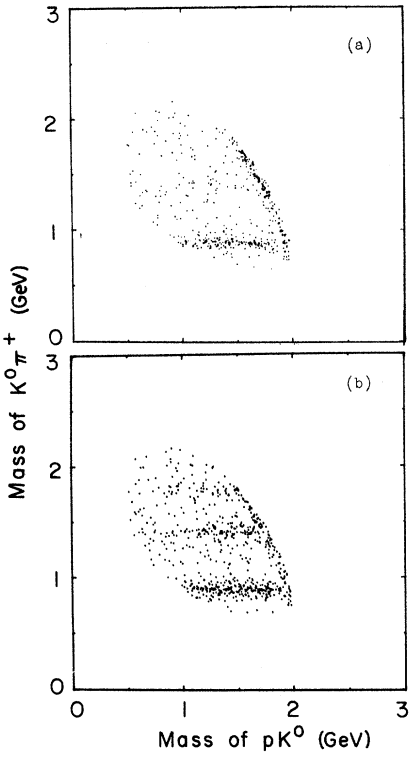


FIG. 35. (a) 4.6-GeV/$c$ scatter plot of data and (b) of theory for $pK^0$ vs $K^0\pi^+$.

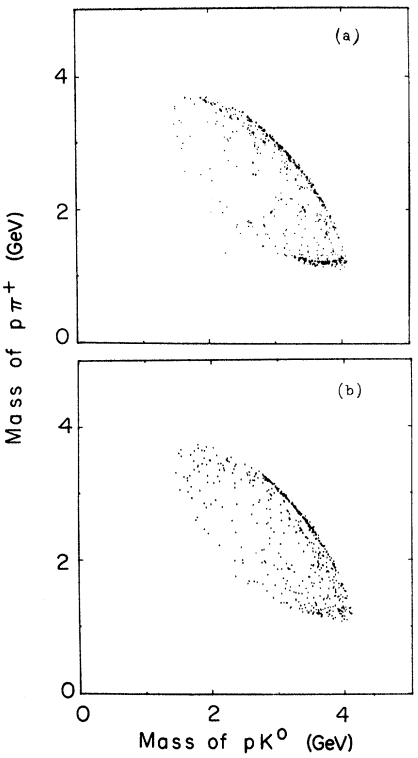


FIG. 37. (a) 9-GeV/$c$ scatter plot of data and (b) of theory for $pK^0$ vs $p\pi^+$.

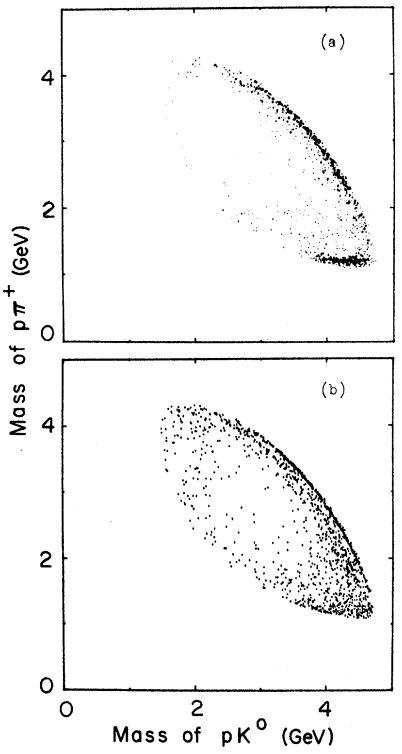


FIG. 36. (a) 12-GeV/$c$ scatter plot of data and (b) of theory for $pK^0$ vs $p\pi^+$.

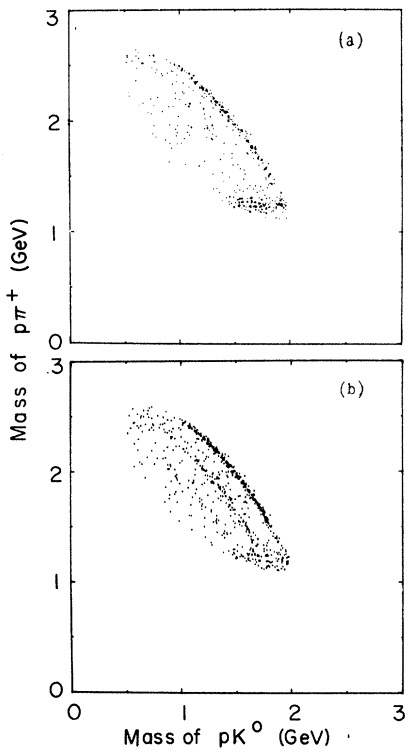


FIG. 38. (a) 4.6 GeV/$c$ scatter plot of data and (b) of theory for $pK^0$ vs $p\pi^+$.

fits are displayed in the figures as well as the regions over which the fits were made. As may be seen, the values of $a$ are in reasonable agreement between the data and the theory. The data appear to be consistently more steeply dipping than the theory. We wish to emphasize that the values of $a$ for the theory are a prediction of the theory once the input trajectories are decided upon.

The angular distributions of the decays of the leading poles in the Jackson frame are not a sensitive test of the theory, since they reflect only the angular momentum structure of the kinematic factor (remember that our trajectories are shifted so that the leading poles are all $l=0$), and there is no daughter structure for the leading poles. The kinematic factor in the $V$ terms in a pure $l=1$. However, since the kinematic factor in the $W$ terms is a mixture of $l=0$ and $l=1$, we see a large $l=0$ contribution to the decay angles of the $K^*(890)$ and $\Delta(1236)$ (Figs. 10, 11, 16, and 17).

The situation is different for the nonleading poles, since here the poles are no longer at $l=0$, and there is an inherent daughter structure apart from the kinematic-term contributions. Unfortunately, the only large nonleading pole in our data is the $K^*(1420)$ (Figs. 13 and 14), for which the data are meager. In any case, although not fitting well, the theory does follow the trend of the data at all energies. The rightmost bin in the $\cos\theta$ histogram is enhanced by the constructive interference of the $K^*(1420)$ with $\Delta(1236)$. The phase of this interference and the approximate magnitude is well predicted by the model.

Figures 30–38 show the Dalitz plots for the data and the theory. Since we only have three particles in the final state, these plots are not independent, but are simply the same information viewed along different projections. We include all the combinations of final-state particles only for completeness. As may be seen, the theory reproduces the features of the Dalitz plot very well at all energies. In viewing these plots, one should make allowances for the fact that the normalization of the theory to the number of events does not match.

### J. Conclusion

We have tested our particular formulation of the generalized Veneziano model at three different energies and have found that the model works equally well at all energies with parameters that vary slowly with energy. We think that for the reaction considered the model is a reasonable one, but we cannot claim that the model will work well in the crossed reactions. Our formulation of pseudoscalar exchange in the $p\bar{p}$ channel does not appear to work well at the lower energies where its effect is significant; however, we are somewhat comforted by the fact that such exchanges have always posed problems in dual models and we expect that our simple formulation was perhaps too optimistic. The model also fails to adequately describe the $p\pi^+$ mass spectrum in the 1.2-GeV mass region, especially in the 4.6-GeV/$c$ data. These failures will probably be amplified if the model is considered for a crossed reaction. There are, however, several successes of the model that are to a large degree independent of the input. Since we think these are positive and interesting results, we list them below.

1. The $K^0\pi^+$ mass spectrum is well fitted and the ratio of $K^*(890)$ to $K^*(1420)$ is excellent; this provides some support for the existence of strong exchange degeneracy between the $K^*$ trajectories.
2. Although the $p\pi^+$ mass spectrum is not impressively fitted, it does not exhibit serious wrong-signature daughter structure or large recurrences.
3. The $K^0p$ mass spectrum is well fitted, supporting the hypothesis for the absence of exotic resonances in this channel.
4. If one ignores the first few bins, the fits to the single-particle $t$ distributions are excellent to the highest value of allowed $t$.
5. Similarly, the $t$ distributions to the $K^*$'s are also good, apart from a slight underestimation of events.
6. The Jackson frame angles of the $K^*(1420)$ are not impressively fitted, but the theory does follow the trend of the data, which is a plus for the model, in view of the fact that the nonleading poles in the theory are rather complex.
7. The Dalitz plot is reproduced very well by the theory. This suggests that the model is reasonable away from the edges of phase space where angular momentum effects are very important.

### ACKNOWLEDGMENTS

We gratefully acknowledge the help we received from A. Barbaro-Galtieri, P. J. Davis, S. E. Derenzo, M. A. Garnjost, G. R. Lynch, M. J. Matison, M. S. Rabin, F. T. Solmitz, and N. M. Uyeda. We thank J. J. Murray for his work in beam design and construction, the Stanford Linear Accelerator 82-in. bubble chamber group for their assistance in data gathering, and the Lawrence Berkeley Laboratory Group A scanning and measuring group for their help in data reduction.

Work done under the auspices of the U. S. Atomic Energy Commission.

*Present address: Lawrence Livermore Laboratory, Livermore, California 94550
†Present address: Department of Physics, University of California, Santa Cruz, California 95060.
‡Present address: Stanford Linear Accelerator Laboratory, Stanford, California 94305.

[1]K. Bardakci and H. Ruegg, Phys. Lett. 18B, 342 (1968).
[2]A. Veneziano, Nuovo Cimento 57, 190 (1968); Chan Hong-Mo and T. S. Tsou, Phys. Lett. 28B, 485 (1969); C. J. Goebel and B. Sakita, Phys. Rev. Lett. 22, 257 (1969).
[3]J. D. Jackson, Rev. Mod. Phys. 42, 12 (1969); D. Sivers and J. Yellin, *ibid.* 43, 125 (1971).
[4]V. Alessandrini, D. Amati, M. LeBellac, and D. Olive, CERN Report No. CERN TH-1160 (unpublished); C. Lovelace, Phys. Lett. 3B, 490 (1970).
[5]B. Petersson and N. A. Tornqvist Nucl. Phys. B13, 629 (1969).
[6]N. A. Tornqvist, Nucl. Phys. B18, 530 (1970).
[7]Chan Hong-Mo, R. O. Raitio, G. H. Thomas, and H. A. Tornqvist, Nucl. Phys. B19, 173 (1970).
[8]J. Bartsch *et al.*, Nucl. Phys. B20, 63 (1970).
[9]R. O. Raitio, Nucl. Phys. B21, 427 (1970); B. Petersson and G. H. Thomas, *ibid.* B20, 451 (1970).
[10]V. Waluch, S. M. Flatté, J. H. Friedman, and D. S. Sivers, Phys. Rev. D 5, 4 (1972).
[11]$K$-82 experiment, Group A, Lawrence Berkeley Laboratory, Berkeley, California.
[12]S. M. Flatté, LBL Group A Physics Note No. 646, 1966 (unpublished).
[13]We use only $\frac{1}{3}$ of the $\chi^2$ that is output by SIOUX from the ionization information provided by the Spiral Reader II. This is because SIOUX forms a $\chi^2$ for each of the three views and outputs the sum. Thus, our factor of $\frac{1}{3}$ is equivalent to assuming that the three views are not independent. Experience has shown that to a fair approximation this is a safe assumption.
[14]The models of Ref. 5 use orderings of the external particles which involve nonplanar Harari-Rosner diagrams. They also omit orderings which involve double-fermion exchange, and this may be related to the use of nonplanar graphs.
[15]P. J. Davis, S. M. Flatté, LBL Group A Physics Note No. 700 (unpublished).
[16]P. J. Davis, S. M. Flatté, LBL Group A Physics Note No. 724 (unpublished).
[17]J. D. Jackson, Nuovo Cimento 34, 1644 (1964).
[18]A. Firestone, G. Goldhaber, D. Lissauer, and G. H. Trilling, Phys. Lett. 36B, 5 (1971).
[19]The absence of diffractive dissociation in $K^*(890)$ production supports the parity rule proposed in Ref. 19.
[20]V. N. Gribov, Yad. Fiz. 5, 197 (1967) [Sov. J. Nucl. Phys. 5, 138 (1967)]; D. R. O. Morrison, Phys. Rev. 165, 1699 (1968).
[21]B. C. Shen, I. Butterworth, Chumin Fu, G. Goldhaber, S. Goldhaber, G. H. Trilling, Phys. Rev. Lett. 17, 569 (1966).
[22]V. Gordon Lind, G. Alexander, A. Firestone, Chumin Fu, G. Goldhaber, Nucl. Phys. B14, 432 (1969).
[23]T. A. Lasinski *et al.*, Rev. Mod. Phys. 45, 1 (1973).
[24]H. Harari, Phys. Rev. Lett. 22, 569 (1970); J. Rosner, *ibid.* 22, 689 (1970).
[25]K. W. Kai and J. Louie, Nucl. Phys. B19, 205 (1970); Auvil, Aalzen, Michael, Weyhis, Phys. Lett. 31B, 303 (1970); Crennell *et al.*, Phys. Rev. Lett. 23, 1347 (1969).
[26]S. Goldhaber *et al.*, Phys. Rev. Lett. 15, 737 (1965).
[27]C. Lovelace, Phys. Lett. 28B, 264 (1968).
[28]J. H. Friedman, J. Comput. Phys. 7, 201 (1971).
[29]We define efficiency as the number of equivalent events divided by the total number of events generated. The number of equivalent events is defined as the sum of the weights of the events squared divided by the sum of the squares of the weights.
[30]J. Hopkinson, DNPL-P-21 report, 1969 (unpublished).
[31]J. H. Friedman, A. Rittenberg, LBL Group A Physics Note No. 171 (unpublished).
[32]CP second stands for central-processor second, a computational unit of time used by the CDC 6600 computer.